



# Independent Validation of the Temperate Super-Earth HD 79211 b using HARPS-N

Victoria DiTomasso<sup>1,18</sup> , Chantanelle Nava<sup>1</sup> , Mercedes López-Morales<sup>1</sup> , Allyson Bieryla<sup>1</sup> , Ryan Cloutier<sup>1</sup> , Luca Malavolta<sup>2</sup> , Annelies Mortier<sup>3,4</sup> , Lars A. Buchhave<sup>5</sup> , Keivan G. Stassun<sup>6</sup> , Alessandro Sozzetti<sup>7</sup> , Aldo Stefano Bonomo<sup>7</sup> , David Charbonneau<sup>1</sup> , Andrew Collier Cameron<sup>8</sup> , Rosario Cosentino<sup>9</sup> , Mario Damasso<sup>7</sup> , Xavier Dumusque<sup>10</sup> , A. F. Martínez Fiorenzano<sup>9</sup> , Adriano Ghedina<sup>9</sup> , Avet Harutyunyan<sup>9</sup> , R. D. Haywood<sup>11,19</sup> , David Latham<sup>1</sup> , Emilio Molinari<sup>12</sup> , Francesco A. Pepe<sup>10</sup> , Matteo Pinamonti<sup>7</sup> , Ennio Poretti<sup>9,13</sup> , Ken Rice<sup>14,15</sup> , Dimitar Sasselov<sup>1</sup> , Manu Stalport<sup>16</sup> , Stéphane Udry<sup>10</sup> , Christopher Watson<sup>17</sup> , and Thomas G. Wilson<sup>8</sup>

<sup>1</sup>Center for Astrophysics | Harvard & Smithsonian, 60 Garden Street, Cambridge, MA 02138, USA; [victoria.ditomasso@cfa.harvard.edu](mailto:victoria.ditomasso@cfa.harvard.edu)

<sup>2</sup>Dipartimento di Fisica e Astronomia “Galileo Galilei,” Università di Padova, Vicolo del l’Osservatorio 3, I-35122 Padova, Italy

<sup>3</sup>KICC & Astrophysics Group, Cavendish Laboratory, University of Cambridge, J.J. Thomson Avenue, Cambridge CB3 0HE, UK

<sup>4</sup>School of Physics & Astronomy, University of Birmingham, Edgbaston, Birmingham, B15 2TT, UK

<sup>5</sup>DTU Space, National Space Institute, Technical University of Denmark, Elektrovej 328, DK-2800 Kgs. Lyngby, Denmark

<sup>6</sup>Department of Physics and Astronomy, Vanderbilt University, Nashville, TN 37235, USA

<sup>7</sup>INAF—Osservatorio Astrofisico di Torino, Via Osservatorio 20, I-10025 Pino Torinese, Italy

<sup>8</sup>Centre for Exoplanet Science, SUPA School of Physics and Astronomy, University of St Andrews, North Haugh, St Andrews KY16 9SS, UK

<sup>9</sup>Fundación Galileo Galilei—INAF, Rambla J.A. F. Perez, 7, E-38712 S.C. Tenerife, Spain

<sup>10</sup>Department of Astronomy, University of Geneva, Chemin Pegasi 51, Versoix, Switzerland

<sup>11</sup>Astrophysics Group, University of Exeter, Exeter EX4 2QL, UK

<sup>12</sup>INAF—Osservatorio Astronomico di Cagliari, Via della Scienza 5, I-09047, Selargius, Italy

<sup>13</sup>INAF—Osservatorio Astronomico di Brera, via E. Bianchi 46, I-23807 Merate (LC), Italy

<sup>14</sup>SUPA, Institute for Astronomy, University of Edinburgh, Blackford Hill, Edinburgh EH9 3HJ, UK

<sup>15</sup>Centre for Exoplanet Science, University of Edinburgh, Edinburgh EH9 3FD, UK

<sup>16</sup>Observatoire de Genève, Université de Genève, 51 ch. des Maillettes, CH-1290 Sauverny, Switzerland

<sup>17</sup>Astrophysics Research Centre, School of Mathematics and Physics, Queen’s University Belfast, Belfast, BT7 1NN, UK

Received 2022 May 25; revised 2022 September 23; accepted 2022 October 18; published 2023 January 6

## Abstract

We present high-precision radial velocities (RVs) from the HARPS-N spectrograph for HD 79210 and HD 79211, two M0V members of a gravitationally bound binary system. We detect a planet candidate with a period of  $24.421^{+0.016}_{-0.017}$  days around HD 79211 in these HARPS-N RVs, validating the planet candidate originally identified in CARMENES RV data alone. Using HARPS-N, CARMENES, and RVs spanning a total of 25 yr, we further refine the planet candidate parameters to  $P = 24.422 \pm 0.014$  days,  $K = 3.19 \pm 0.27$  m s<sup>-1</sup>,  $M \sin i = 10.6 \pm 1.2 M_{\oplus}$ , and  $a = 0.142 \pm 0.005$  au. We do not find any additional planet candidate signals in the data of HD 79211, nor do we find any planet candidate signals in HD 79210. This system adds to the number of exoplanets detected in binaries with M-dwarf members and serves as a case study for planet formation in stellar binaries.

*Unified Astronomy Thesaurus concepts:* [Exoplanet detection methods \(489\)](#); [Radial velocity \(1332\)](#); [M dwarf stars \(982\)](#); [Binary stars \(154\)](#)

*Supporting material:* machine-readable tables

## 1. Introduction

M dwarfs are the most common stars, constituting as many as 75% of the stars in our Galaxy (Henry et al. 2006), and every M dwarf is predicted to host at least one planet (Dressing & Charbonneau 2015). The abundance of M dwarfs and the prevalence of planets around them, combined with the relatively large signals planets impose on low-mass stars, have made M dwarfs the primary target for many exoplanet studies. Previous studies report that between 23% and 46% of M dwarfs are in binaries (Ward-Duong et al. 2015; Winters et al. 2019; Susemihl & Meyer 2022), but so far only about 30 exoplanets (less than 7% of the total found around M dwarfs) have been

found around binaries where at least one member is an M dwarf. Approximately 20 planets have been found orbiting M-dwarf components in an S-type configuration, characterized by the planet orbiting around just one star in a binary, around M-dwarf components (Thebault & Haghighipour 2015), and less than 10 circumbinary planets have been found around binaries with an M-dwarf member (e.g., Doyle et al. 2011; Orosz et al. 2012; Schwamb et al. 2013; Jain et al. 2017). Hundreds of exoplanets have been, and will continue to be, discovered around M dwarfs, allowing for studies of planet formation in binaries with M-dwarf members.

HD 79210 and HD 79211 are a pair of M0V stars that comprise a gravitationally bound binary. These two stars are, in many ways, twins. They are nearly identical in mass, radius, and effective temperature according to literature measurements (see Table 1), varying by only a few percent at most. Together they form one of only ten stellar binary exoplanet host systems with a binary mass ratio greater than 0.9. With a period of  $1295 \pm 180$  yr and a semimajor axis of  $130.9 \pm 5.1$  au (González-Álvarez et al. 2020), these stars have a projected

<sup>18</sup> National Science Foundation Graduate Research Fellow.

<sup>19</sup> STFC Ernest Rutherford Fellow.



**Table 1**  
Stellar Parameters for HD 79210 and HD 79211 Found in the Literature

Parameter	HD 79210	HD 79211	References
R.A. (deg)	138.5835616152243	138.5913117966687	Gaia Collaboration et al. (2016)
decl. (deg)	52.68408016691263	52.68342944184038	Gaia Collaboration et al. (2016)
Spectral type	M0V	M0V	Alonso-Floriano et al. (2015)
Distance (pc)	$6.332 \pm 0.002$	$6.332 \pm 0.002$	Gaia Collaboration et al. (2012)
Parallax (mas)	$157.8879 \pm 0.0197$	$157.8825 \pm 0.0211$	Gaia Collaboration et al. (2012)
$\mu_\alpha \cos \delta$ (mas a <sup>-1</sup> )	$-1545.787 \pm 0.018$	$-1573.040 \pm 0.018$	Gaia Collaboration et al. (2012)
$\mu_\delta$ (mas a <sup>-1</sup> )	$-569.053 \pm 0.018$	$-659.906 \pm 0.019$	Gaia Collaboration et al. (2012)
$U$ (km s <sup>-1</sup> )	$-42.20 \pm 0.36$	$-44.01 \pm 0.36$	Cortes-Contreras et al. (2016)
$V$ (km s <sup>-1</sup> )	$-14.99 \pm 0.10$	$-17.44 \pm 0.10$	Cortes-Contreras et al. (2016)
$W$ (km s <sup>-1</sup> )	$-23.73 \pm 0.34$	$-23.10 \pm 0.34$	Cortes-Contreras et al. (2016)
Eff. temp., $T_{\text{eff}}$ (K)	$4001 \pm 100^*$	$4014 \pm 100^*$	Sarmiento et al. (2021)
	$4024 \pm 51$	$4005 \pm 51$	Schweitzer et al. (2019)
Surface grav, $\log g$ (cgs)	$4.68 \pm 0.07$	$4.68 \pm 0.07$	Schweitzer et al. (2019)
Metallicity, [M/H] (dex)	$4.71 \pm 0.1$	$4.63 \pm 0.1$	Sarmiento et al. (2021)
Metallicity, [Fe/H]	$-0.05 \pm 0.16$	$-0.03 \pm 0.16$	Schweitzer et al. (2019)
Luminosity ( $L_\odot$ )	$0.0789 \pm 0.0038$	$0.0792 \pm 0.0031$	Schweitzer et al. (2019)
Mass ( $M_\odot$ )	$0.69 \pm 0.07^*$	$0.64 \pm 0.07^*$	González-Álvarez et al. (2020)
	$0.591 \pm 0.047$	$0.596 \pm 0.042$	Schweitzer et al. (2019)
Radius ( $R_\odot$ )	$0.58 \pm 0.02$	$0.58 \pm 0.03$	Schweitzer et al. (2019)
$v \sin i$ (km s <sup>-1</sup> )	$2.9 \pm 1.2$	$2.3 \pm 1.5$	Glebocki & Gnacinski (2005); Reiners et al. (2018)
$P_{\text{rot}}$ (days)	$16.3^{+3.5}_{-1.3}$	$16.61 \pm 0.04$	González-Álvarez et al. (2020)
Age (Gyr)	1–7	1–7	González-Álvarez et al. (2020)
$v_{\text{mic}}$ (km s <sup>-1</sup> )	4.71	4.63	Sarmiento et al. (2021)
$v_{\text{mac}}$ (km s <sup>-1</sup> )	-0.06	-0.11	Sarmiento et al. (2021)

**Note.** These are the values that we ultimately use for fitting the radial velocities and deriving the parameters of the planet candidate. In the cases where multiple values are listed for a single parameter, \* denotes the value adopted in this work.

separation of 108.54 au and a semimajor axis of 130 au (González-Álvarez et al. 2020). Many studies of disk evolution as well as exoplanet formation and occurrence around binary stars cite 100 au either projected separation or semimajor axis as a boundary for various behaviors. For example: binaries with separations greater than 100 au do not seem to affect planet populations, in comparison to single stars (Desidera & Barbieri 2007; Mugrauer & Neuhauser 2009; Kraus et al. 2016); closer binaries (<100 au separation) are less likely to host planets (Roell et al. 2012; Bergfors et al. 2013; Kraus et al. 2016); and planets in wide binaries ( $100 \text{ au} < a < 700 \text{ au}$ ) tend to have inclinations that are aligned with those of the stellar binary (Christian et al. 2022). With only around 4% of all exoplanet-hosting stars being members of binary or multiple systems (Marzari & Thebault 2019), the HD 79210/HD 79211 binary system serves as a valuable edge-case data point for these binary planet population studies.

While no transiting planet has yet been detected around either of these targets, González-Álvarez et al. (2020) published a radial-velocity (RV) detection of a planet candidate around HD 79211 using high-precision radial velocities from the CARMENES spectrograph (Quirrenbach et al. 2016). They reported a planet with an orbital period of  $24.45 \pm 0.02$  days, a semimajor axis of  $0.141 \pm 0.005$  au, a semi-amplitude of  $3.07 \pm 0.37 \text{ m s}^{-1}$ , and a minimum mass of  $10.27^{+1.47}_{-1.38}$  or  $9.97^{+1.47}_{-1.38} M_\oplus$ , depending on their adopted stellar mass. They found one significant periodic signal in the RV data of HD 79210 at 16.3 days, which they attributed to the stellar rotation period.

In this paper, we search for a 24.4 day planet with a period of 24.4 days around HD 79211 in the HARPS-N data taken as part of the HARPS-N GTO Rocky Planet Search (RPS) program, as well as in High Resolution Echelle Spectrometer

(HIRES) data from Butler et al. (2017), in an effort to support this planet’s presence and refine its parameters. We also look for additional signals in the HARPS-N, HIRES, and CARMENES data of both targets. In Section 2, we discuss the data used throughout this paper. In Section 3, we discuss our efforts to characterize the two stars. In Section 4, we share our analysis of the new photometric light curves taken with KeplerCam. In Section 5, we present our RV analysis, and in Section 6 we report our results and discussion.

## 2. Data

### 2.1. HARPS-N Spectroscopy and White Light Radial Velocities

These two targets were observed using the HARPS-N spectrograph installed on the 3.6 m Telescopio Nazionale Galileo (TNG) at the Observatorio del Roque de los Muchachos in La Palma, Spain (Cosentino et al. 2012; Cosentino 2014). HARPS-N is an updated version of HARPS at the ESO 3.6 m telescope (Mayor et al. 2003), with a proven RV stability of better than  $1 \text{ m s}^{-1}$ .

There are a total of 81 observations of HD 79210 taken between 2014 January and 2022 March (Figure B1). There are a total of 114 observations of HD 79211 taken between 2012 December and 2022 March (Figure 1). Both objects were observed as part of the HARPS-N guaranteed time observation (GTO) Rocky Planet Search program. The aim of this program is to monitor the radial velocities of nearby, bright, quiet stars in search of low-mass planets orbiting them (Motalebi et al. 2015). For this program, targets were observed with exposure times to minimize the effect of stellar noise with short typical timescales, i.e., averaging out p-mode oscillations (Chaplin et al. 2019). Additional measurements of the targets are spaced by two or five hours during the night to minimize the effect of

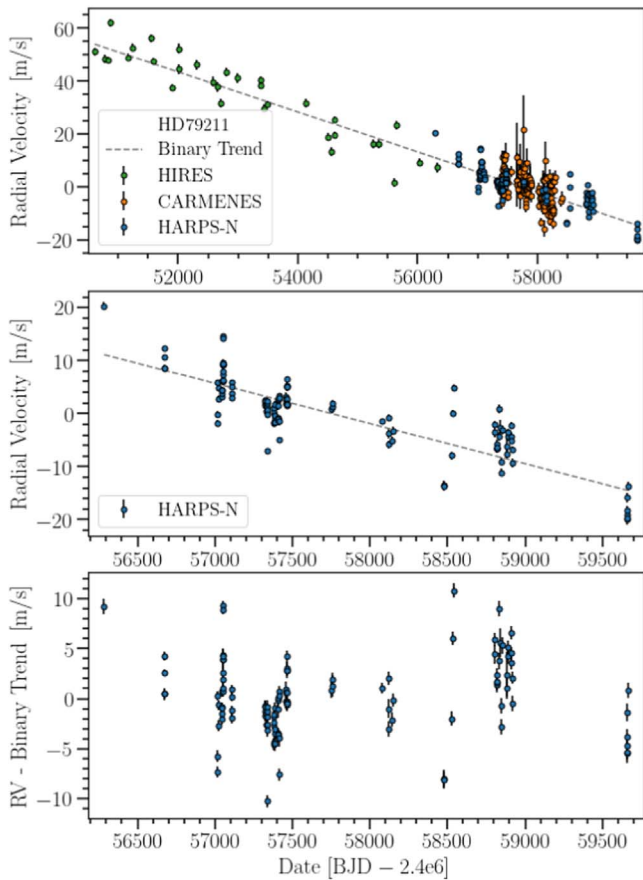


**Figure 1.** Radial velocities for HD 79211 measured from CARMENES (orange, top panel only), HARPS-N (blue, all panels), and HRES (green, top panel only) spectra. For most data points, the uncertainty in the RV is smaller than the size of the point. We mark the binary trend, fit as a second-order polynomial, with a dashed line in the top and middle panels. The bottom panel shows the HARPS-N radial velocities with the binary trend subtracted. We use the HARPS-N RVs with the binary trend removed when calculating the correlation between RV and activity indicators (Figure 4), and when calculating periodograms (Figures 5, 6, 7, 8).

granulation (Dumusque et al. 2011; Pepe et al. 2011; Motalebi et al. 2015).

These spectra were reduced with version 3.7 of the HARPS-N Data Reduction Software (DRS, Pepe et al. 2011). This pipeline calculates the spectral bisector inverse slope (BIS), FWHM, and contrast, as well as each observation’s  $H\alpha$ , Na-Index, and Mount Wilson S-index,  $S_{MW}$ . We included all of the above values in our analysis as stellar activity indicators.

We calculated radial velocities from these spectra using the HARPS-TERRA software, which calculates radial velocities using a spectral template derived from the observations themselves, and has been shown to be particularly effective when applied to M dwarfs (see Anglada-Escudé & Butler 2012 for more information). The resulting RV measurements have median uncertainties of  $0.65 \text{ m s}^{-1}$  for HD 79210 and  $0.62 \text{ m s}^{-1}$  for HD 79211.

## 2.2. HARPS-N Chromatic Radial Velocities

We also used the HARPS-N spectra to calculate chromatic radial velocities for HD 79211 to test the potential effect of stellar activity. We divided the spectra into three wavelength ranges, 383.0–446.89 nm, 443.26–513.87 nm, and 510.39–690 nm, and then calculated the RV of the target

based on each spectral range independently. This procedure is explained in detail in Mortier et al. (2020) and summarized here. We coadded all of the CCFs calculated using version 3.7 of the HARPS-N Data Reduction Software (DRS) from each echelle order that belonged to the desired wavelength range, and performed a Gaussian fit on the result in order to obtain the corresponding chromatic RV. We estimated the RV error from the photon noise, the total counts of the coadded CCFs, and the read-out noise. We applied a correction factor to the noise estimate in order to closely reproduce the RV error from the full-spectrum CCF, knowing that the chromatic RVs will inevitably be noisier than the full-spectrum RVs. The average error on the full-spectrum HARPS-N DRS RVs for both targets was  $0.56 \text{ m s}^{-1}$ , and the median error on the chromatic RVs determined by each spectral range was  $2.35 \text{ m s}^{-1}$ ,  $1.14 \text{ m s}^{-1}$ , and  $0.99 \text{ m s}^{-1}$ , respectively. Note that these chromatic radial velocities were calculated using the CCFs from the HARPS-N DRS, not using the HARPS-TERRA software like the white light RVs used in the rest of this work.

## 2.3. Absolute Astrometry

The Gaia EDR3 archive reports two statistical indicators of possible deviations from a single-star solution that might indicate the presence of orbiting companions, *astrometric\_excess\_noise* and RUWE (renormalized unit weight error). The values of the two parameters are 0.127 mas, 1.08 and 0.138 mas, 1.11, for HD 79210 and HD 79211, respectively. The values of *astrometric\_excess\_noise* are in line with those obtained for very bright stars, for which the calibration of Gaia astrometry will require further improvements. The RUWE values are clearly below the empirical threshold of 1.4 above which the single-star solution is deemed unsatisfactory (Lindgren et al. 2018, 2021), and which might be an indication of the presence of an unresolved companion. A more stringent threshold at  $\text{RUWE} \gtrsim 1.1$  has been proposed in recent studies (Belokurov et al. 2020; Stassun & Torres 2021) for the identification of unresolved stellar systems, but this is better used for selection of samples rather than a single source basis. The historical RV and astrometric time series (see González-Álvarez et al. 2020, and references therein) do not show obvious evidence of additional, massive unresolved companions orbiting either HD 79210 or HD 79211. We finally note that astrometric acceleration catalogs such as those from Kervella et al. (2022) and Brandt (2021) show statistically significant (signal-to-noise ratio  $> 10$ ) proper-motion anomalies at the mean Gaia epoch for both components. This information can be used to further improve the constraints on the binary orbit, but such a study goes beyond the scope of this paper.

## 2.4. Previously Published High-precision Radial Velocities

There are 70 high-precision RV measurements of HD 79210 and 159 of HD 79211 published in González-Álvarez et al. (2020). These measurements were obtained with the VIS channel of the CARMENES spectrograph on the 3.5 m telescope of the Calar Alto Observatory (Quirrenbach et al. 2016). The observations were taken from 2016 March to 2019 January and 2016 January to 2018 October, respectively, with median uncertainties of  $2.2$  and  $2.0 \text{ m s}^{-1}$ , respectively. González-Álvarez et al. (2020) also published near-infrared RVs, but with uncertainties averaging  $9 \text{ m s}^{-1}$ , they did not

have high enough precision to search for the  $\approx 3 \text{ m s}^{-1}$  signal at 24.4 days.

We also include 32 radial velocities of HD 79210 that were obtained between 1997 June and 2013 December with a median uncertainty of  $1.27 \text{ m s}^{-1}$ , and 32 radial velocities of HD 79211 that were obtained between 1997 June and 2013 February with a median uncertainty of  $1.53 \text{ m s}^{-1}$  using the HIRES spectrograph (Vogt et al. 1994) on the Keck telescope (Butler et al. 2017). With only one to a few data points per season, these RVs are not sufficient to constrain any planet candidate orbital parameters on their own, but are used in our analysis where we include them as additional points alongside the HARPS-N and CARMENES radial velocities.

### 2.5. Photometric Light Curves

HD 79210 and HD 79211 are bright M dwarfs in a binary, and are separated by  $17''$  on the sky. Because of this small angular separation, these two targets are blended in many photometric surveys, such as ASAS-SN (Shappee et al. 2014; Kochanek et al. 2017), WASP (Pollacco et al. 2006), and TESS (Ricker et al. 2015). González-Álvarez et al. (2020) did obtain optical photometric time series of the two stars, but lacking adequate reference stars, calculated their differential photometry using each member of the binary as a reference for the other. Ultimately, they were not able to attribute any photometric variability to one star or the other. Because of this, we collected new light curves for these two targets.

We obtained new photometric light curves for both HD 79210 and HD 79211 with the aim of determining their stellar rotation periods. We took images using the KeplerCam wide-field CCD camera on the 1.2 m telescope at the Fred Lawrence Whipple Observatory (FLWO) on Mount Hopkins, Arizona. The  $4096 \times 4096$ ,  $15 \mu\text{m}$  pixels format provides a  $23.1$  square field of view with a resolution of  $0.338$  per pixel (Szentgyorgyi et al. 2005), and our images were binned by two.

From 2021 February until 2021 June, we took a total of 6081 images of HD 79210 and HD 79211 using the *B*-band filter on KeplerCam. The exposure time of each image was 2 s. We reduced the raw images, first by stitching together the four individual images from each quadrant of the detector (Carter et al. 2011) and then performing bias subtraction and flat-field correction. We performed photometry using AstroImageJ (AIJ; Collins et al. 2017). We used AIJ’s variable radius, multi-aperture photometry function, by which AIJ determines the aperture radius from an azimuthally averaged radial profile, centered on the user-defined aperture. It then determines the net integrated counts within the object aperture, as well as the average value of the pixels in the user-defined sky annulus, not including background pixels that are more than two sigma above the average background pixel value (Collins et al. 2017), and returns the difference between those values as the Source-Sky counts. AIJ also calculates an error value on the Source-Sky counts, which includes contributions from read-out noise, dark current, and source and sky Poisson noise as defined by Merline & Howell (1995).

We used AIJ to calculate the Source-Sky counts and error on those measurements for our two targets, HD 79210 and HD 79211, as well as three comparison stars found within the field: HD 233614, HD 79450, and TYC 3806-1026-1. We present three sets of relative photometry: that of HD 79210 calculated using TYC 3806-1026-1 as a comparison star, that of HD 79211 calculated using TYC 3806-1026-1 as a comparison

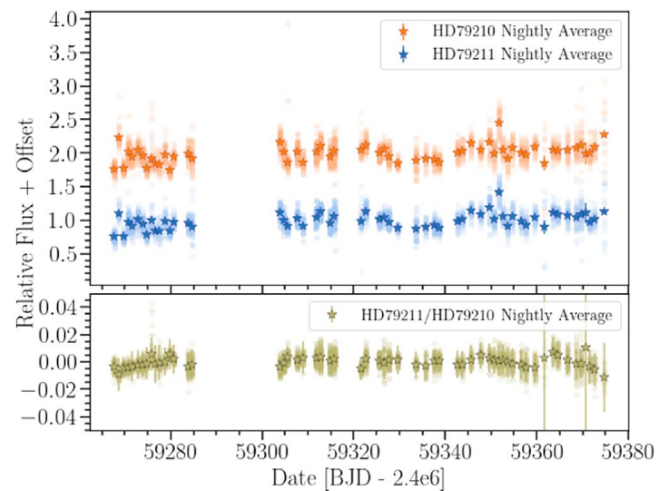


**Figure 2.** Relative photometry for HD 79210 using a comparison star (orange), relative photometry for HD 79211 using a comparison star (blue), and relative photometry for HD 79211 using HD 79210 as a comparison star (green), plus an offset, as taken with KeplerCam. Note the different y-axis scale between the two separate light curves in the upper panel and the combined light curve in the lower panel. The faint, round points represent the relative flux measurement from each individual image. The darker, star-shaped points represent the nightly averaged relative flux. These average nightly fluxes are what we used when calculating the periodograms (Figure 3). These two separate light curves are highly affected by systematics, which we discuss in detail in Section 4.

star, and that of HD 79211 calculated using HD 79210 as a comparison star (see Section 4 for more information). We opted to combine the multiple exposures taken over the course of the night into nightly measurements. The resulting light curves, after sigma clipping outlier points, are shown in Figure 2.

### 2.6. Literature Photometry

As with the time-series surveys discussed in Section 2.5, HD 79210 and HD 79211 are blended in many past photometric surveys as well, due to their small separation on the sky. In some surveys, such as that of the Wide-field Infrared Survey Explorer (WISE), these two stars are blended beyond separability. We opt not to quote the magnitudes for the blended source here. In other surveys, such as the Galaxy Evolution Explorer (GALEX), Two Micron All-Sky Survey (2MASS), and the Sloan Digital Sky Survey (SDSS), the photometric values suffer from some amount of blending or diffraction spike confusion, which has been corrected in post-processing, and magnitudes for these objects are reported in those survey catalogs. In even higher angular resolution surveys, namely Hipparcos and Tycho, Gaia, and USNO, the two stars are resolved. We have listed all available photometric values in Table B1, noting those that come from surveys in which the two stars were originally blended.

## 3. Stellar Characterization

The HD 79210/HD 79211 binary is located 6.332 pc from Earth (Gaia Collaboration et al. 2012). These two stars are very similar to one another and are in many ways twins. They are nearly identical in mass, radius, and effective temperature according to literature measurements (see Table 1), varying by only a few percent at most. HD 79210 had been classified as a K7V star (Kirkpatrick et al. 1991), but more recently has been classified as an M0V star, like HD 79211 (Alonso-Floriano et al. 2015).

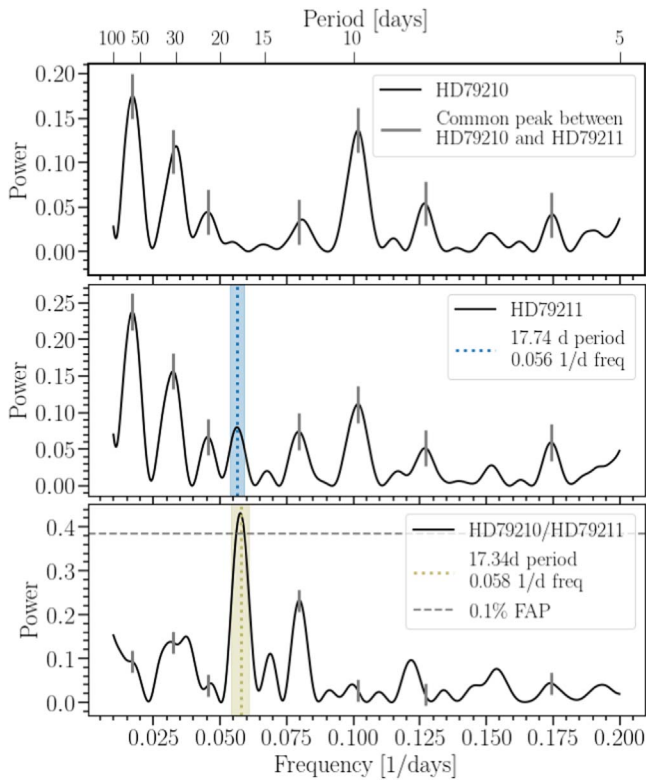


**Figure 3.** Lomb–Scargle periodogram of the nightly averaged relative fluxes for HD 79210 using a separate comparison star (top), HD 79211 using a separate comparison star (middle) and HD 79210 as a comparison star (bottom). The vertical, gray dashes note the shared peaks between the two stars’ periodograms, which are likely caused by systematics in the images. The statistically significant ( $<0.1\%$  FAP) peak in the bottom periodogram is marked with the dotted green line, and the shaded region marks one standard deviation around the peak ( $P = 17.34$  days,  $\text{freq} = 0.057 \pm 0.003 \text{ day}^{-1}$ ). This peak corresponds to the one peak in HD 79211’s periodogram that is not present in that of HD 79210, marked with the blue dotted line in the middle panel, at 17.74 days ( $\text{freq} = 0.056 \pm 0.003 \text{ day}^{-1}$ ). Although the 17.74 days peak is not statistically significant, this suggests that this photometric variability originates in HD 79211, and we attribute it to this star’s rotation period.

In Table 1, we summarize the previously published parameters for these two stars. For the majority of the parameters, we cite the same sources used by González-Álvarez et al. (2020), with one addition. These two stars have since been included in Sarmento et al. (2021)’s sample of 313 M-dwarf stars, for which they derived  $T_{\text{eff}}$  and metallicity using *H*-band APOGEE spectra.

For our investigation, we attempted a number of different methods to calculate the stellar parameters for the two stars in this system, namely Stellar Parameter Classification (SPC; Buchhave et al. 2012, 2014), isochrone fitting (Morton 2015; Mortier et al. 2020), empirical color–parameter relations (Boyajian et al. 2012; Mann et al. 2015; Benedict et al. 2016), and spectral energy distribution (SED) fitting (Stassun & Torres 2016). Ultimately, we decide to use the literature values for the stellar parameters (Table 1) in our analysis, for the following reasons. SPC does not produce reliable results for these targets as they are at the edge of the range of stellar effective temperatures for which SPC is calibrated. The isochrone-fitting procedure takes the SPC-derived effective temperature and metallicity as inputs, as well as the flagged 2MASS photometry, making the isochrone results similarly unreliable. HD 79210 and HD 79211 fall at or beyond the

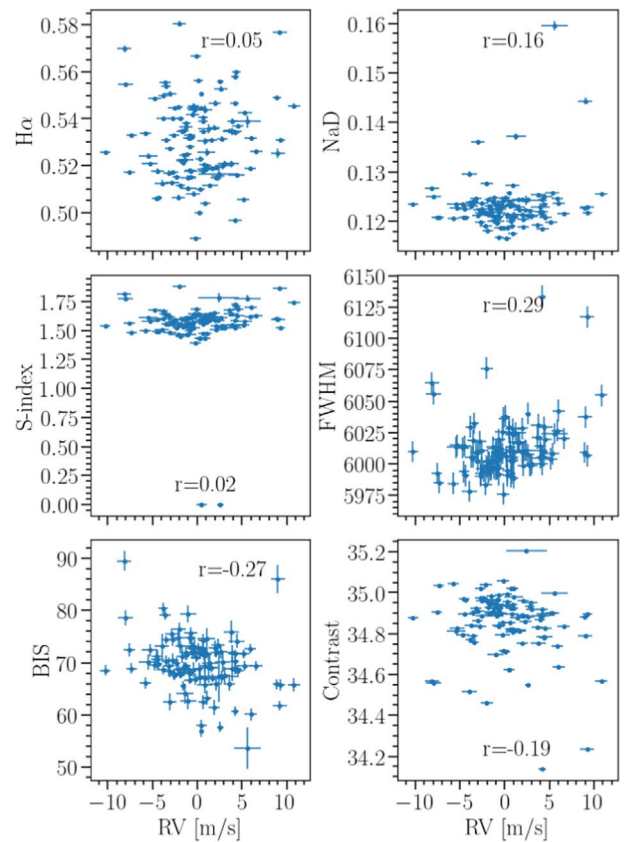


**Figure 4.** Various HARPS-N stellar activity indicators versus HD 79211’s radial velocities after the stellar binary trend has been subtracted. The  $r$ -values are Pearson correlation coefficients. All of these parameters are weakly correlated, with  $r$ -values less than 0.3.

upper range of stellar masses, depending on the true mass of the stars, for which the mass–luminosity relationship (Boyajian et al. 2012) was calibrated. The color–temperature relationship (Mann et al. 2015) also relies on the flagged 2MASS photometry.

Finally, we determined the stellar masses, radii, and effective temperatures via spectral energy distribution (SED) fitting, following the procedure in Stassun & Torres (2016). These results were the least consistent with the other methods and the previously published values, finding that the stars are cooler and more metal-poor, and have larger radii than otherwise measured. This could have an astrophysical origin: low-mass stars in much tighter, eclipsing binaries ( $P < 10$  days) have been shown to have larger radii and cooler temperatures than predicted by models. Current theory explains that tidal effects between the two members of the binary cause the stars to rotate quickly and be more active. Either through magnetic fields suppressing convective energy transport or high spot coverage lowering the average temperature of the stellar surface and forcing a larger radius to conserve energy, the stars end up being larger and cooler than otherwise predicted (Ribas et al. 2008 and the references therein). These stars’ wide binary separation, lack of evidence of fast rotation, and other activity indicators not pointing toward them being extremely active, however, do not support this explanation of radius inflation and temperature suppression. More likely, the contamination between the stars in their photometry is causing an unreliable SED fit. For these reasons, we decide not to report the stellar parameters determined using these various methods, and opt

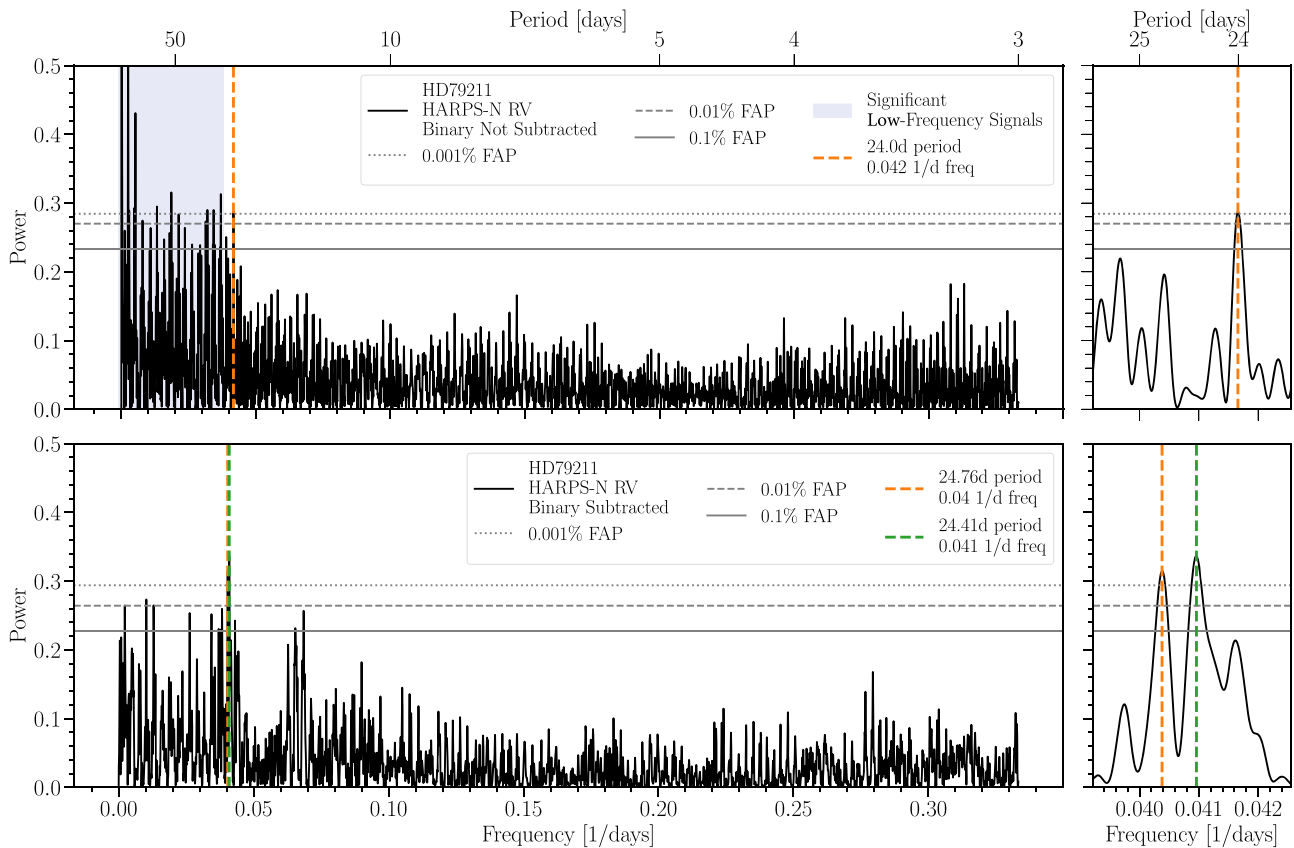


**Figure 5.** Periodograms of HARPS-N radial velocities of HD 79211, without the binary trend removed (top) and with the binary trend removed (bottom). Signals with frequencies from 0 to  $0.33 \text{ day}^{-1}$  are plotted. Signals with False Alarm Probabilities of less than 0.1% are marked. Before the binary trend is removed, there are many significant low-frequency signals (blue shaded region), as we would expect from the long-period binary. Two signals with FAPs of less than 0.01% are marked for HD 79211 once the binary trend is removed, at 24.41, and 24.76 days. The signal at 24.41 days is attributed to the planet candidate and has the highest power of the present peaks.

use the literature values for the stellar parameters (Table 1) in our analysis.

#### 4. Light-curve Analysis

We present three sets of relative photometry for these stars: that of HD 79210 calculated using TYC 3801-1026-1 as a comparison star, that of HD 79211 calculated using TYC 3801-1026-1 as a comparison star, and that of HD 79211 calculated using HD 79210 as a comparison star. There were three comparison stars in the field of our observations, all of which are at least two orders of magnitude fainter than the target stars ( $B$  magnitudes of 9.92, 9.33, and 11.55 in comparison to HD 79211’s  $B$  magnitude of 7.966) and are different spectral types (all are F stars, as opposed to the targets, which are M0; Høg et al. 2000). We decided to use TYC 3801-1026-1 as our comparison star when calculating the separate relative photometry for HD 79210 and HD 79211 because it best corrected for the effect of changing airmass over the course of our observations.

There were a number of nights of observations that we opted not to use from our KeplerCam photometric measurements. The seven nights of observation between 2021 March 21 and 29 were significantly offset in both relative and absolute flux from the rest of the nights’ fluxes for both targets, likely due to moon contamination. Since we were not able to correct for this offset in the relative photometry using the available comparison stars, we decided to exclude these nights from our analysis.

We also opted not to use two other nights, 2021 April 4 and 13, because the seeing changed significantly over the course of the night, resulting in unreliable flux measurements.

The resulting light curves from the two stars (Figure 2, in orange and blue) and their periodograms (Figure 3, upper two panels) clearly show the influence of systematics. Even by eye, the time variations of these two light curves appear to be identical, indicating that they are the results of systematics affecting the images from which both stars’ light curves were reduced. We rule out the far less likely scenario that the two stars were undergoing identical variation during the time of our observations. Due to the available comparison stars being bluer and fainter than our targets, these systematics persist despite using other stars in the field for calibration.

Although the other stars in the field are poorly suited comparisons for HD 79210 and HD 79211, each target serves as an ideal comparison for the other, because of their similar masses, shared spectral type, and close proximity on the sky. We calculated relative photometry of HD 79211 using HD 79210 as a comparison (Figure 2, in green), which corrects for the systematics found in the other light curves. A periodogram of this combined light curve shows a statistically significant ( $<0.1\%$  FAP) peak at a period of 17.34 days and frequency of  $0.057 \pm 0.003 \text{ day}^{-1}$  (Figure 3, bottom panel). Alone, we cannot attribute this periodicity to one star or the other. A nearby peak, however, at 17.74 days/ $0.056 \pm 0.003 \text{ day}^{-1}$  is present in the periodogram of HD 79211’s separate light curve but not in HD 79210’s separate light curve. Although this

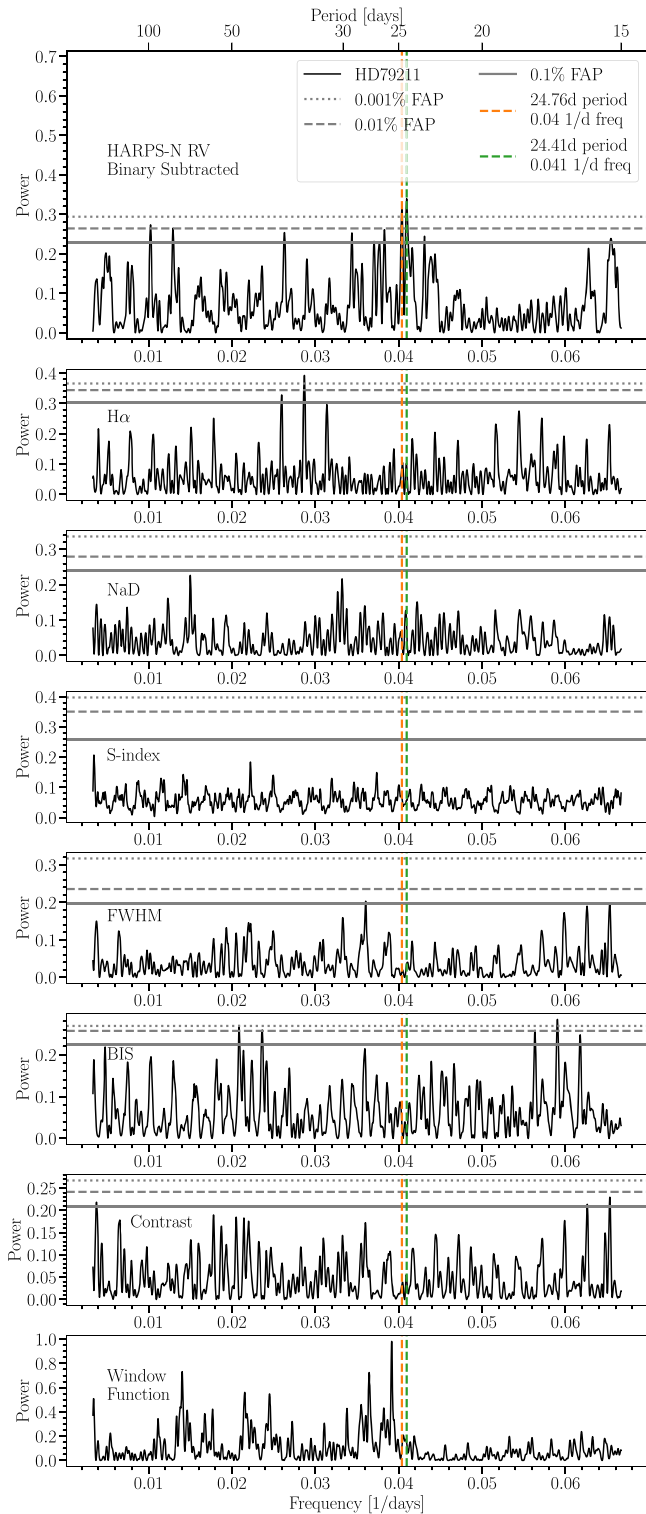


**Figure 6.** Periodograms of HD 79211’s white light HARPS-N radial velocities with the binary trend removed, activity indicators, and the window function. All of significant peaks ( $<0.01\%$  FAP) are marked with dashed vertical lines. The most significant peak is at 24.41 days, which we attribute to the planet candidate. We attribute the other significant peak, at 24.76 days, to aliases of the planet candidate signal (see Figure 7).

17.74 days peak is not statistically significant, its presence suggests that this approximately 17.5 days periodicity originates in HD 79211’s photometric variability. We attribute this variability to HD 79211’s rotation period.

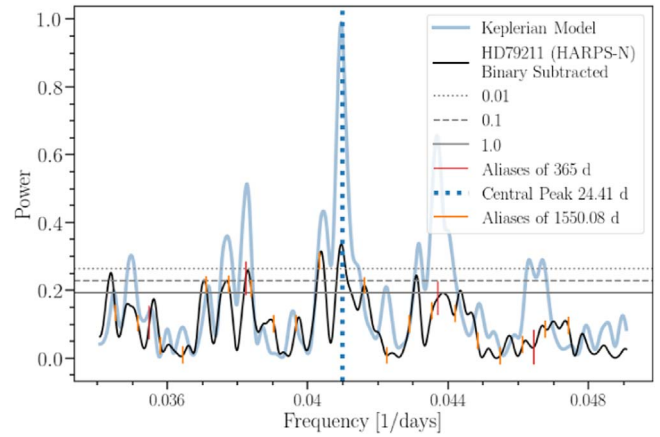


**Figure 7.** Zoomed-in periodogram of the HD 79211 white light HARPS-N RVs, highlighting the strongest peak in the periodogram at 24.41 days and the aliases that result in its interaction with the 365 and 1550.8 day peaks in the window function. The periodogram calculated from the best-fit Keplerian planet orbit, sampled with the observing cadence of the HARPS-N data, is plotted in light blue. There is variation between the periodograms of the model and the data, but much of the aliasing structure can be seen in both periodograms. The 24.76 day peak (above the 0.01% FAP line) can be explained as an alias.

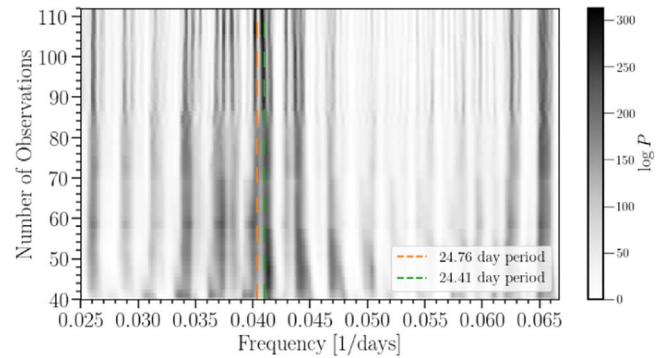


**Figure 8.** Stacked Bayesian Generalized Lomb–Scargle periodograms (SBGLS) for the HD 79211 HARPS-N white light radial velocities, with the binary trend removed. The horizontal axis is the frequency of the signal, the color is the power, and the vertical axis shows how the periodogram changes as observations are added to the calculation. This periodogram is oversampled by a factor of 5. The same peaks are highlighted from the 2D periodogram; Figure 6. The strongest peak at 24.41 days gets stronger as more observations are added, as we would expect for a planet signal.

## 5. Radial-velocity Analysis

### 5.1. Stellar Binary Trend Removal

The stellar binary, with its 1300 yr period and nearly  $1 \text{ km s}^{-1}$  amplitude, introduces a significant RV trend to HD 79210 and HD 79211. Following González-Álvarez et al. (2020), we tried approximating the stellar binary trend as a line, but found that a line fit did not capture the curvature introduced by extending our RV time baseline with the addition of the HIRES and HARPS-N data sets. We ultimately opted for modeling the stellar binary as a second-order polynomial, fit to the combined HARPS-N, CARMENES, and HIRES data set (Figures 1 and B1). In order to find correlations between the HARPS-N RVs and the various activity indicators (Section 5.2), and calculate periodograms of the radial velocities (Sections 5.3, 5.4), we subtracted offsets between these three data sets and the binary polynomial trend. We used

**Table 2**  
RV Fits for Three Sets of HD 79211 RVs Using PyOrbit

Parameter	Prior	HARPS-N Only $e = 0$	HARPS-N Only $e < 0.3$	HARPS-N + CARMENES $e = 0$	HARPS-N + CARMENES <sup>a</sup> $e < 0.3$	HARPS-N + CARMENES + HIRES $e = 0$	HARPS-N + CARMENES + HIRES $e < 0.3$
<b>Planet Orbit</b>							
$P_b$ (days)	U: 10–50	$24.426^{+0.015}_{-0.016}$	$24.421^{+0.016}_{-0.017}$	$24.425^{+0.013}_{-0.014}$	$24.422 \pm 0.014^a$	$24.438^{+0.009}_{-0.012}$	$24.435^{+0.011}_{-0.019}$
$K_b$ (m s <sup>-1</sup> )	U: 0.01-10	$3.68 \pm 0.50$	$3.71^{+0.52}_{-0.51}$	$3.19 \pm 0.27$	$3.19 \pm 0.27^a$	$3.14 \pm 0.27$	$3.14 \pm 0.27$
$e_b$	Varies	$\equiv 0.0$	$0.142^{+0.113}_{-0.100}$	$\equiv 0.0$	$0.109^{+0.100a}_{-0.075}$	$\equiv 0.0$	$0.097^{+0.096}_{-0.067}$
$T_{\text{conj}_b}$ (JD – 2.4e6)	G: 57,517.06 ± 6.15	$57,522.08^{+0.52}_{-0.54}$	$57,521.72^{+1.02}_{-1.38}$	$57,521.99^{+0.35}_{-0.36}$	$57,521.43^{+0.72a}_{-0.90}$	$57,521.81 \pm 0.35$	$57,521.34^{+0.66}_{-0.83}$
<b>Derived</b>							
$a_b$ (au)	...	$0.142 \pm 0.005$	$0.142 \pm 0.005$	$0.142 \pm 0.005$	$0.142 \pm 0.005^a$	$0.142 \pm 0.005$	$0.142 \pm 0.005$
$M_b \sin i(M_{\oplus})$	...	$12.3^{+2.0}_{-1.9}$	$12.3^{+2.0}_{-1.8}$	$10.7 \pm 1.2$	$10.6 \pm 1.2^a$	$10.6 \pm 1.2$	$10.4 \pm 1.2$
<b>Gaussian Process</b>							
$H_{\text{amp}}$ HN (m s <sup>-1</sup> )	...	$4.00^{+0.82}_{-0.65}$	$4.03^{+0.85}_{-0.68}$	$3.79^{+0.77}_{-0.62}$	$3.74^{+0.76a}_{-0.62}$	$3.70^{+0.75}_{-0.61}$	$3.67^{+0.74}_{-0.61}$
$H_{\text{amp}}$ CAR (m s <sup>-1</sup> )	...	...	...	$3.71^{+0.94}_{-0.70}$	$3.75^{+0.97a}_{-0.71}$	$3.70^{+0.95}_{-0.70}$	$3.72^{+0.96}_{-0.72}$
$H_{\text{amp}}$ HIRES (m s <sup>-1</sup> )	...	...	...	...	...	$5.16^{+1.57}_{-2.36}$	$5.23^{+1.54}_{-2.44}$
$P_{\text{dec}}$ (days)	U: 15–1000	$180^{+69}_{-68}$	$197^{+89}_{-76}$	$200^{+47}_{-40}$	$203^{+49a}_{-43}$	$209^{+49}_{-43}$	$213^{+51}_{-45}$
$P_{\text{rot}}$ (days)	U: 16.419-18.623	$16.70^{+0.22}_{-0.09}$	$16.75^{+0.29}_{-0.12}$	$16.60 \pm 0.05$	$16.58^{+0.05a}_{-0.06}$	$16.59 \pm 0.05$	$16.59 \pm 0.05$
$O_{\text{amp}}$	G: 0.5 ± 0.05	$0.48 \pm 0.05$	$0.48 \pm 0.05$	$0.46 \pm 0.05$	$0.46 \pm 0.05^a$	$0.46 \pm 0.05$	$0.46 \pm 0.05$
<b>Binary Trend</b>							
c1:	...	$-0.01 \pm 0.001$	$-0.01 \pm 0.001$	$-0.009 \pm 0.001$	$-0.01 \pm 0.001^a$	$-0.002 \pm 0.001$	$-0.009 \pm 0.001$
c2 (e-07):	...	$-1.86^{+1.14}_{-1.17}$	$-1.94^{+1.13}_{-1.16}$	$-1.04^{+1.23}_{-1.25}$	$-1.06^{+1.21a}_{-1.26}$	$-.46^{+1.33}_{-1.40}$	$-.54^{+1.35}_{-1.45}$
x zero (JD – 2.4e6):	...	57,773.91	57,871.94	57,871.94	57,871.94 <sup>a</sup>	57,773.91	57,773.91
<b>Offset and Jitter</b>							
Off HN (m s <sup>-1</sup> ):	...	$0.63^{+1.25}_{-1.12}$	$-0.38^{+1.26}_{-1.14}$	$-0.59^{+1.13}_{-1.09}$	$-0.61^{+1.12a}_{-1.07}$	$0.22^{+1.14}_{-1.10}$	$0.23^{+1.12}_{-1.09}$
Off CAR (m s <sup>-1</sup> ):	...	$0.81 \pm 0.37$	$-0.20 \pm 0.36$	$-0.19^{+1.51}_{-1.50}$	$-0.17^{+1.54a}_{-1.52}$	$0.72^{+1.52}_{-1.50}$	$0.74^{+1.55}_{-1.52}$
Off HIRES (m s <sup>-1</sup> ):	...	$-46.49 \pm 2.59$	$-47.59^{+2.64}_{-2.67}$	$-45.93^{+2.81}_{-2.90}$	$-46.06^{+2.86a}_{-2.82}$	$-45.42^{+3.19}_{-3.21}$	$-45.43^{+3.17}_{-3.23}$
Jit HN (m s <sup>-1</sup> ):	...	$1.47^{+0.20}_{-0.19}$	$1.49^{+0.20}_{-0.19}$	$1.51^{+0.20}_{-0.18}$	$1.53^{+0.20a}_{-0.19}$	$1.54^{+0.20}_{-0.18}$	$1.55^{+0.20}_{-0.18}$
Jit CAR (m s <sup>-1</sup> ):	...	$3.88^{+0.30}_{-0.28}$	$3.88^{+0.30}_{-0.28}$	$1.66 \pm -0.28$	$1.64 \pm 0.28^a$	$1.67 \pm 0.28$	$1.65^{+0.28}_{-0.27}$
Jit HIRES (m s <sup>-1</sup> ):	...	$5.60^{+0.91}_{-0.73}$	$5.58^{+0.89}_{-0.72}$	$5.63^{+0.89}_{-0.73}$	$5.63^{+0.90a}_{-0.73}$	$3.02^{+2.13}_{-1.88}$	$2.99^{+2.16}_{-1.91}$

**Note.** We fit HARPS-N RVs alone, HARPS-N + CARMENES RVs, and HARPS-N + CARMENES + HIRES RVs with both eccentric and circular orbits. We adopt the results of fitting the HARPS-N + CARMENES RVs with an eccentric orbit as our final results. U in the prior column denotes a Uniform prior and G denotes a Gaussian prior.

<sup>a</sup> Adopted fit values.

RadVel to fit for these offsets and binomial parameters (Fulton et al. 2018).

When fitting the RVs to find the planetary parameters, we chose to fit a polynomial trend (to model the binary trend), a Keplerian (to model the planet), and Gaussian processes (GPs; to model stellar activity) simultaneously. We did this using PyOrbit (Malavolta 2016), which allows the user to specify which data sets are used to fit which models—allowing us to fit the binary trend using the combined HARPS-N, HIRES, and CARMENES data sets, while varying which data sets contributed to the Keplerian and GP fits (Section 5.5).

## 5.2. HARPS-N RV Correlation with Stellar Activity Signatures

The HARPS-N stellar activity indicators were calculated as described in Section 2.1. We calculate the Pearson correlation coefficients ( $r$ ) for the HARPS-N radial velocities and activity indicators using SciPy’s `pearsonr` function (Oliphant 2007) for HD 79210 and HD 79211 (Figures B2 and 4, respectively). We define a moderate correlation as  $0.5 > r \geq 0.3$  and a weak correlation as  $r < 0.3$ . HD 79211’s radial velocities are weakly correlated with all activity indicators. Radial velocities from

HD 79210, however, are moderately correlated with FWHM and weakly correlated with the rest.

## 5.3. Periodograms of the White Light HARPS-N RVs

Periodograms of the HARPS-N RVs of HD 79210 and HD 79211 with the binary trend removed, calculated using Astropy’s `LombScargle` function (Price-Whelan et al. 2018), are shown in Figures 5 and B3. The False Alarm Probabilities (FAPs) are calculated via bootstrap simulations. The periodogram of HD 79211’s radial velocities reveals signals with less than 0.01% FAP at the following periods: 24.41 and 24.76 days. The signal at 24.41 days is the most significant and we attribute it to the planet candidate. When plotted with the periodograms of the various stellar activity indicators and the window function (Figure 6), we see that these signals in the RV periodograms do not correspond with peaks in any of the stellar activity indicators. We attribute the other significant peak, at 24.76 days, to an alias of the 1550 day peak in the window function interacting with the 24.41 day peak (Figure 7). Aliases can appear in periodograms at frequencies equal to the true frequency of a signal, in this



case  $1/24.4$  days, plus or minus the frequency in the window function caused by the data sampling, in this case  $1/1550$  days. We support this interpretation by plotting the periodogram of the best-fit Keplerian planetary orbit over that of the data with the binary trend removed in Figure 7. While the uncertainty of the data and the effects of stellar activity prevent the model and data periodograms from matching precisely, this shows that we are capable of detecting a 24.42 day signal with the observing cadence of our data, and that many of the aliases in our data correspond to those in the model. The periodogram of HD 79210’s RVs, after the binary trend is subtracted, does not reveal any signals with less than a 0.01%.

We also present the stacked Bayesian General Lomb–Scargle periodogram (Figure 8, calculated via the procedure in Mortier & Collier Cameron 2017). This stacked periodogram shows that the 24.41 day signal becomes stronger as more observations are added, as we would expect for a planet signal. We also note that the approximately 24.4 day periodic signal is present in the periodogram of HD 79211’s RVs regardless of how we corrected for the binary trend, whether as a line, Keplerian, or as a second-order polynomial, as we are showing here. We suspect that the stellar rotation period is not present as a significant signal in these periodograms because, over the course of the observations, the magnetically active regions of the star evolved such that the stellar rotation fell out of phase.

#### 5.4. Periodograms of the Chromatic HARPS-N RVs

The significant peaks from the periodograms of the white light HARPS-N radial velocities are also highlighted in the periodograms of the chromatic radial velocities (Figure 9). Both signals from the white light RVs are present in these chromatic periodograms, with increasing significance as we look to the redder RVs. Because this signal is not larger in the bluer wavelengths, as we would expect if the signal were caused by stellar activity, we do not take this as clear evidence that the 24.41 day signal is caused by stellar activity. We investigate the variation in the amplitude of the 24.41 day signal by fitting each set of chromatic radial velocities using PyOrbit and discuss those results in Section 5.5.1.

#### 5.5. Radial-velocity Fits

To determine the planetary parameters, we fit the radial velocities via a Markov Chain Monte Carlo (MCMC) fitting routine using PyOrbit (Malavolta 2016). We fit the data with a second-order polynomial to model the stellar binary, a Keplerian to model the planet candidate, and GPs to model stellar activity, as well as offset and jitter parameters for all of the data sets. As described in Section 2.1, we simultaneously fit a second-order polynomial (to model the binary trend) to the combined HARPS-N, CARMENES, and HIRES data sets, while fitting GPs (to model the stellar activity), and a Keplerian (to model the planet) to various combinations of the three data sets. We used this procedure to fit for a planet signal in the data of HD 79210 and HD 79211, but were not able to identify any planet candidates in the HD 79210 data. In this section, we present the resulting best-fit parameters for the planet candidate around HD 79211.

Using PyOrbit (Malavolta 2016), we fit the HARPS-N RVs of HD 79211 with the priors described in the Appendix

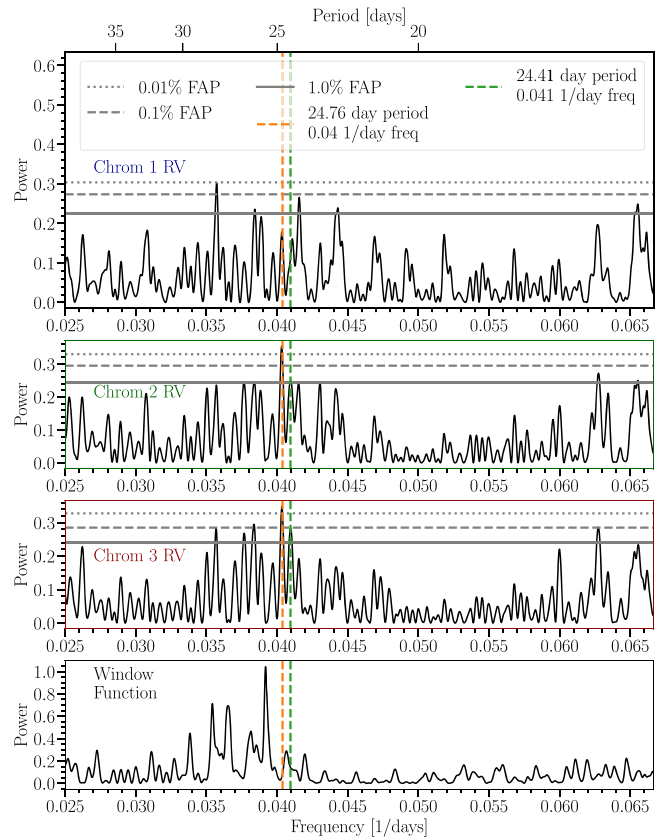


**Figure 9.** Periodograms of the three chromatic HARPS-N RV sets and the window function. The top panel shows chrom1 RVs (calculated using the bluest portion of the spectrum), followed by chrom2, and chrom3 in the lowest RV panel (calculated using the reddest portion of the spectrum). The window function is shown in the white light bottom panel. The same significant peaks that are marked in the white light RV periodogram (Figure 6) are marked here with vertical dashed lines. Both signals are present in these chromatic periodograms, with increasing significance as we look to the redder RVs. Because this signal is not larger in the bluer wavelengths, as we would expect if the signal were caused by stellar activity, we do not take this as evidence that the 24.41 day signal is caused by stellar activity.

(Section A). We performed similar fits for HD 79210 and were not able to find any planet signals. We report the results of six fits for HD 79211: fitting just the HARPS-N radial velocities, fitting the combined HARPS-N + CARMENES RVs, and fitting the combined HARPS-N + CARMENES + HIRES RVs, with both a circular and an eccentric orbit and with Gaussian processes to model stellar activity. The priors and results of our fits to the RVs from HD 79211 can be found in Table 2 and the phase-folded best-fit models are shown in Figure 10. The results of all of these runs are consistent within their quoted uncertainties.

We adopt the results of fitting the HARPS-N + CARMENES data set with an eccentric orbit as our final results for the planet candidate around HD 79211 (full posteriors shown in Figure B5). This is the model favored by an AIC model comparison. Although the results of fitting the combination of all three data sets are consistent with those of fitting the HARPS-N + CARMENES data set, an aliasing effect caused by a peak in the window function that is unique to the HARPS-N + CARMENES + HIRES data set causes the posterior of the planet period to be double peaked, at 24.44 and 24.38 days. Ultimately, we identify a signal with a period of

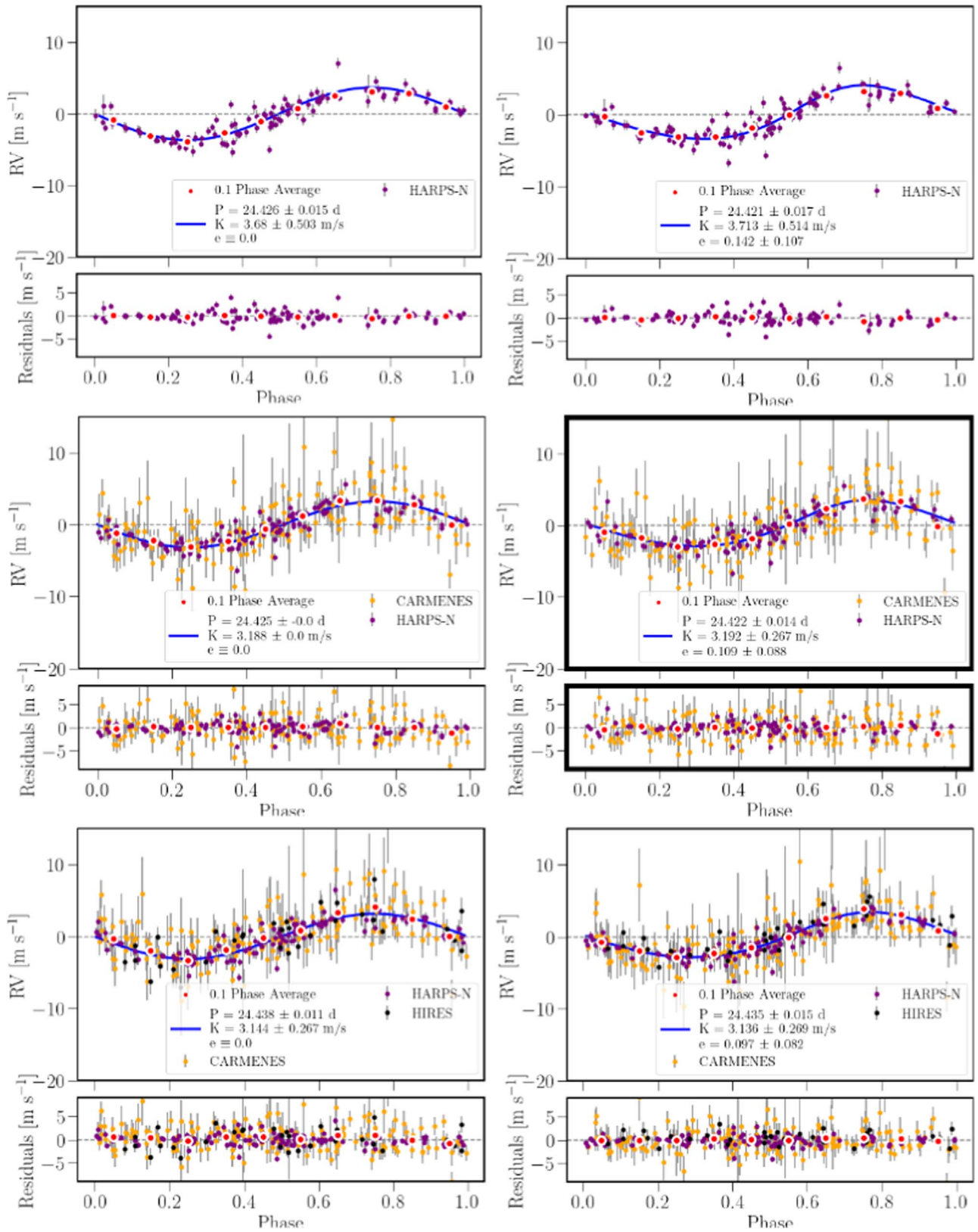


**Figure 10.** Phase-folded, best-fit Keplerian orbital model, after the Gaussian processes and binary star trend have been removed, as well as their residuals. The top row shows the best-fit model to the HARPS-N data alone, the middle row shows the combined HARPS-N + CARMENES data set, and the bottom row shows the HARPS-N + CARMENES + HIRES data set. The left-hand column shows the circular fits to these data sets and the right-hand column shows the corresponding eccentric fits. The blue line is the best-fit model with the orbital parameters printed in the legend and listed in Table 2. Red circles are the same velocities binned in 0.1 units of orbital phase. The middle right-hand panel, marked with a bold border, shows our final, adopted parameters for the planet candidate.

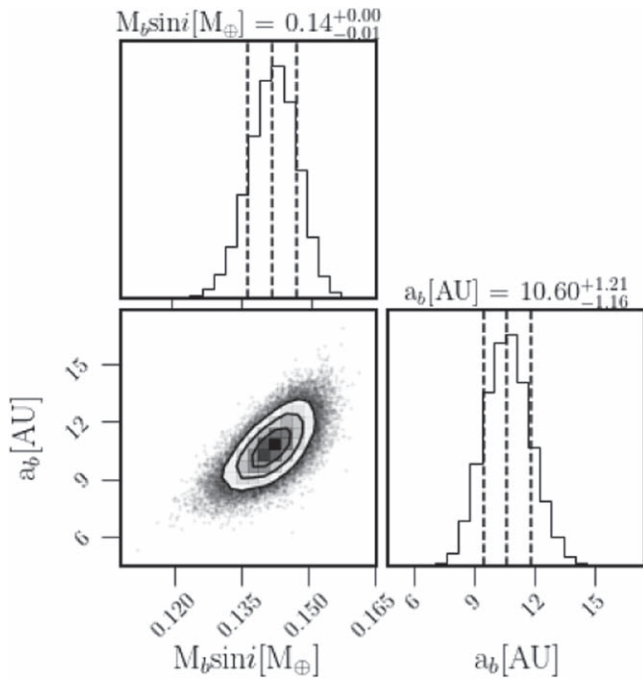


**Figure 11.** Posterior distributions of the combined HARPS-N and CARMENES data set for HD 79211b’s parameters derived from fitting an eccentric orbit.

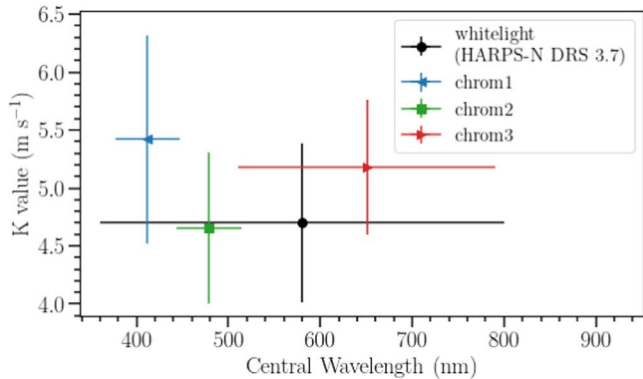


**Figure 12.** We fit the chromatic radial velocities using RadVel, fixing all of the parameters and hyperparameters except for  $K_b$  to the best-fit values found from fitting the white light HARPS-N DRS RVs (the white light counterpart to the chromatic RVs), not the HARPS-TERRA RVs that we use in the rest of this work. Here, we plot the resulting  $K_b$  versus the wavelength band used to calculate those radial velocities. The white light RV result from fitting the HARPS-N DRS RVs is noted by the black point. All of these values agree within their error bars, and they do not show the trend of increasing semiamplitude with decreasing wavelength that we would expect of a signal caused by stellar activity.

$24.422 \pm 0.014$  days and attribute it to a planet candidate orbiting HD 79211, with an  $M \sin i$  of  $10.6 \pm 1.2 M_{\oplus}$  and  $a = 0.142 \pm 0.005$  au (Figure 11).

We also fit the chromatic RVs (described in Section 2.1) using RadVel, to see if the semiamplitude of the signal in HD 79211 varies with the wavelength of light used to calculate the radial velocities. Fixing the parameters and hyperparameters except for  $K_b$  (i.e.,  $P_b$ ,  $e_b$ ,  $T_{\text{conj}}$ ,  $H_{\text{amp}}$ ,  $P_{\text{dec}}$ ,  $P_{\text{rot}}$ ,  $O_{\text{amp}}$ ,  $\sigma_{\text{HN}}$ ,  $c1$ ,  $c2$ ,  $x$  zero) to the best-fit values found from fitting the white light HARPS-N DRS RVs, we fit the chromatic light curves and compare their semiamplitudes. Note that we used the

HARPS-N RVs as calculated by the DRS, not by HARPS-TERRA, to find these parameters. These results are shown in Figure 12. We found that the semiamplitudes were consistent, within error bars, across the chromatic RV sets and in comparison to the white light semiamplitude. Although we caution against overinterpreting these results, we could expect stellar activity to cause stronger signals in bluer light and smaller signals in redder light, whereas we expect a planet signal to be consistent across colors.

## 6. Results and Discussion

We present the results of analyzing HARPS-N, CARMENES, and HIRES radial velocities from HD 79210 and HD 79211. We ultimately conclude that there likely is a planet orbiting HD 79211, with a period of  $24.422 \pm 0.014$  days, semiamplitude of  $3.19 \pm 0.27 \text{ m s}^{-1}$ ,  $M \sin i = 10.6 \pm 1.2 M_{\oplus}$ , and  $a = 0.142 \pm 0.005$  au, and we find no evidence of any planet candidates around HD 79210.

There are discrepancies between the periodograms of HD 79211’s radial velocities from HARPS-N alone (Figure 5) and CARMENES alone (González-Álvarez et al. 2020). Periodograms of the CARMENES RVs show three peaks significant above the 0.1% FAP level at 8.3, 24.4, and 16.6 days, explained by González-Álvarez et al. (2020) as a harmonic of the stellar rotation period, the planet’s orbital period, and the stellar rotation period, respectively. The periodograms of the HARPS-N RVs, however, show two significant peaks above the 0.01% FAP level at 24.41 and 24.76 days. We suspect that these discrepancies are caused by the fluctuation in stellar activity between seasons. Due to the low time-density of HARPS-N data, however, we are not able to isolate the HARPS-N data from the seasons where the two data sets overlap in order to perform a direct comparison.

All of our RV fits (Table 2) found a periodic signal at  $\approx 24.4$  days, with all parameters agreeing within their error bars. Ultimately, this work supports the detection of the 24.4 day planet candidate around HD 79211 originally published by González-Álvarez et al. (2020), and finds no additional candidates around either HD 79211 or its binary companion HD 79210. As discussed in that work, this planet candidate is one of the lowest-mass planets discovered orbiting one member of a stellar binary with a semimajor axis below 400 au. It likely lies on the inner edge of its star’s habitable zone, but it is likely nontransiting, with only a  $5_{-1}^{+2}\%$  chance that it is transiting (González-Álvarez et al. 2020). Even so, with these two stars’ borderline-wide separation of  $a = 130$  au, this system can serve as a valuable data point in future studies of exoplanet formation and occurrence around stellar binaries.

This material is based upon work supported by the National Science Foundation Graduate Research Fellowship under grant No. DGE1745303. The HARPS-N project was funded by the Prodex Program of the Swiss Space Office (SSO), the Harvard-University Origin of Life Initiative (HUOLI), the Scottish Universities Physics Alliance (SUPA), the University of Geneva, the Smithsonian Astrophysical Observatory (SAO), the Italian National Astrophysical Institute (INAF), University of St. Andrews, Queen’s University Belfast, and University of Edinburgh. Parts of this work have been supported by the National Aeronautics and Space Administration under grant

No. NNX17AB59G, issued through the Exoplanets Research Program. Parts of this work have been supported by the Brinson Foundation. R.D.H. is funded by the UK Science and Technology Facilities Council (STFC)’s Ernest Rutherford Fellowship (grant No. ST/V004735/1). T.G.W and A.C.C acknowledge support from STFC consolidated grant Nos. ST/R000824/1 and ST/V000861/1, and UKSA grant ST/R003203/1. This work has made use of data from the European Space Agency (ESA) mission Gaia (<https://www.cosmos.esa.int/gaia>), processed by the Gaia Data Processing and Analysis Consortium (DPAC, <https://www.cosmos.esa.int/web/gaia/dpac/consortium>). Funding for the DPAC has been provided by national institutions, in particular the institutions participating in the Gaia Multilateral Agreement.

## Appendix A

### Selection of Priors for Radial-velocity Fits

When fitting for a planet candidate around HD 79211, we used the time of conjunction for the 24.4 day planet candidate published in González-Álvarez et al. (2020) as our Gaussian prior ( $2457517.06 \pm 6.15$  days). We ran both circular-orbit fits and eccentric fits. We started with a wide prior on eccentricity ( $e < 0.8$ ), but found that it favored highly eccentric and physically unlikely orbits, resulting from fitting a gap in data with the peak RV. We then narrowed to  $e < 0.3$ . We kept the prior on our semiamplitude ( $K_b$ ) wide throughout our fits, with a Jeffery’s prior from  $0.01$  to  $10 \text{ m s}^{-1}$ .

We initially set a wide, uniform prior on orbital period (3–50 days), which resulted in a double-peaked posterior, with one peak tending toward the lower end of this prior range and another at around  $\approx 25$  days. After constraining the orbital period to the lower range, we found that the lower peak resulted from the code trying to fit a one-day periodic signal that originates in the window function. We then opted to increase the lower bound of our orbital period prior (uniform prior from 10 to 50 days), preventing the MCMC from fitting that one-day periodicity.

In our fits using Gaussian processes to model stellar activity, we used a quasi-periodic kernel with four hyperparameters: variability amplitude ( $H_{\text{amp}}$ ), nonperiodic characteristic length (associated with the spot decay timescale,  $P_{\text{dec}}$ ), variability period (associated with the stellar rotation period,  $P_{\text{rot}}$ ) and periodic characteristic length (associated with the number of spots/spot regions on the surface of the star,  $O_{\text{amp}}$ ).

We set a wide uniform prior on  $P_{\text{dec}}$  from 15.0 to 1000.0 days. The lower limit is associated with the approximate lower limit on the estimated rotation period of the star, since if the stellar magnetically active regions are evolving more quickly than the star is rotating, we would not see a periodic signal at all. The upper limit is many times the rotation period of the star, to allow for a fit to stable, long-lived magnetically active regions on the star.

We then set a uniform prior on  $P_{\text{rot}}$  from 16.419 to 18.623 days, restricting this value to the one standard deviation range around the peaks in the periodograms of the light curves for HD 79211 (see Section 4). We set a Gaussian prior of  $0.5 \pm 0.05$  on  $O_{\text{amp}}$  (Jeffers & Keller 2009; Haywood et al. 2018). This accounts for the fact that the photometric and RV variability effect of even highly complex spot distributions on a star will average out to those caused by two or three large spots on the visible surface of the star.

When fitting the chromatic HARPS-N radial velocities, we aim to detect differences in the semiamplitude of the periodic signal at the suspected planet’s period. To do this, we decided to fix all of the free parameters— $T_{\text{conj}}$ ,  $P_b$ ,  $H_{\text{amp}}$ ,  $P_{\text{dec}}$ ,  $P_{\text{rot}}$ ,  $O_{\text{amp}}$ ,  $c_1$ ,  $c_2$ ,  $x$  zero—to the best-fit values returned from fitting the white light HARPS-N DRS and CARMENES joint data set. Note that, for this step, we used the HARPS-N RVs as calculated by the DRS (which are the white light counterpart to the chromatic radial velocities), and not those calculated by HARPS-TERRA, to find these parameters. Although we do expect the chromatic nature of stellar activity to cause changes in the amplitude of the stellar activity signal ( $H_{\text{amp}}$ ) between chromatic sets of RV data, we opted to fix this value in order to remove the degeneracy between the change in amplitude induced by stellar activity and by the planet candidate.

## Appendix B Figures

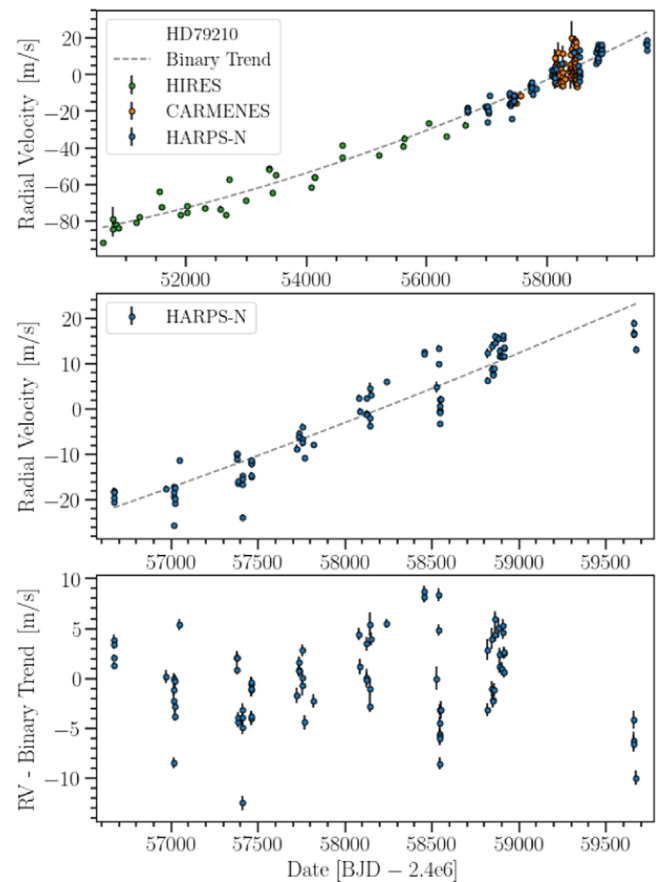


**Figure B1.** Radial velocities for HD 79211 measured from CARMENES (orange, top panel only), HARPS-N (blue, all panels), and Hires (green, top panel only) spectra. For most data points, the uncertainty in the RV is smaller than the size of the point. We mark the binary trend, fit as a second-order polynomial, with a dashed line in the first and third panels. The bottom panel shows the HARPS-N radial velocities with the binary trend subtracted. We use the HARPS-N RVs with the binary trend removed in our periodograms and when calculating correlation with stellar activity indicators analysis (Figures B2, B3, B4).

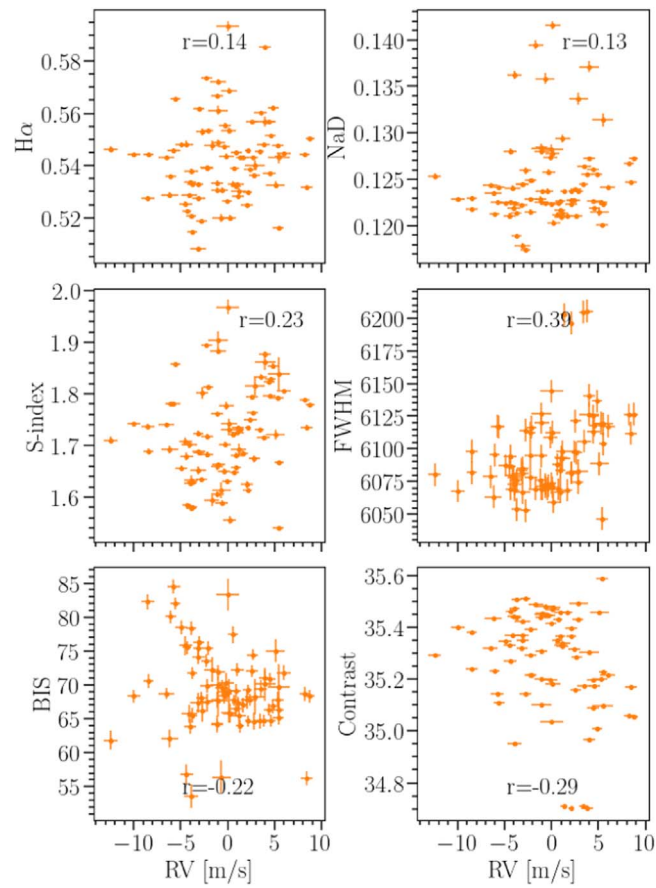


**Figure B2.** Various HARPS-N stellar activity indicators versus HD 79210's radial velocities after the stellar binary trend has been subtracted. The  $r$ -values are Pearson correlation coefficients. FWHM is moderately correlated, with an  $r$ -value of 0.39.

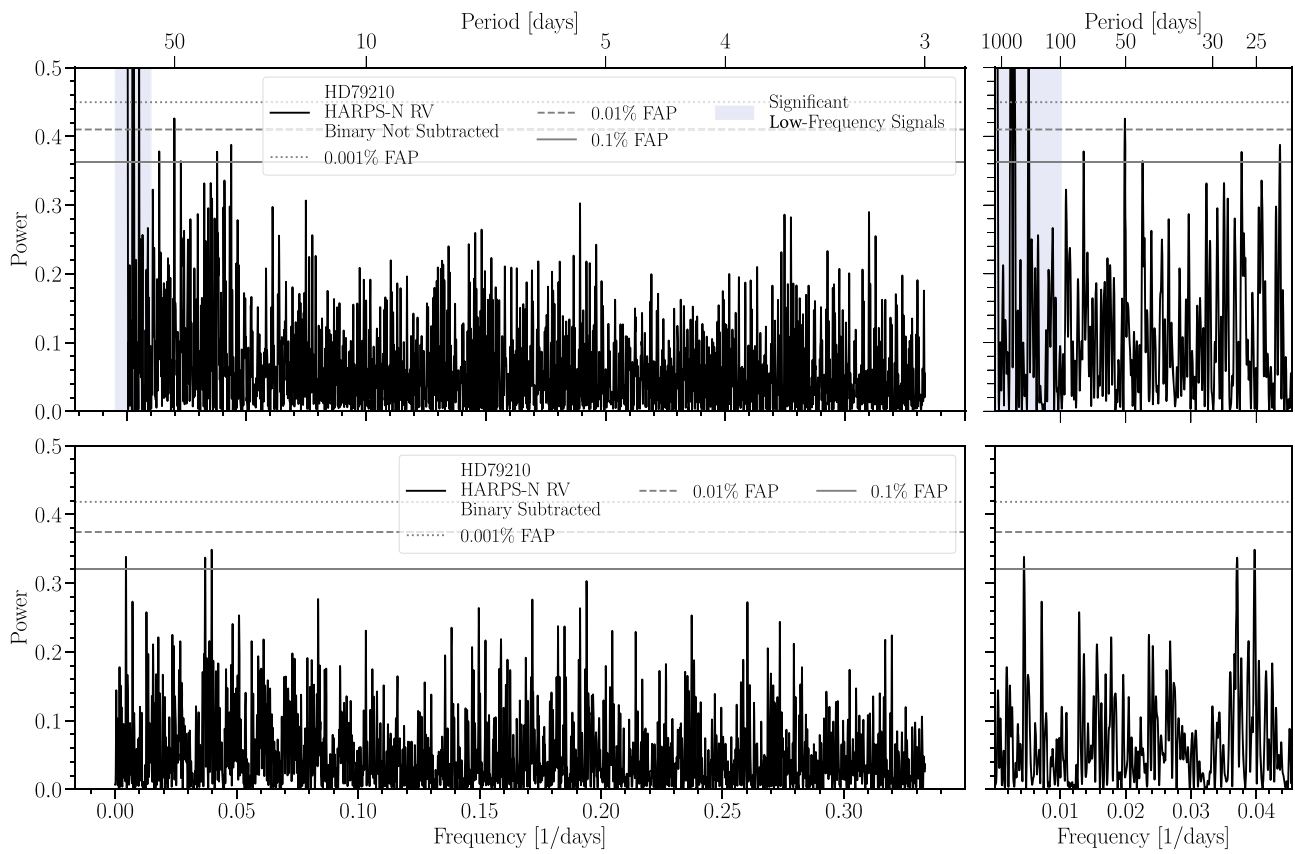


**Figure B3.** Periodograms of HARPS-N radial velocities of HD 79210, without the binary trend removed (top) and with the binary trend removed (bottom). Signals with frequencies from 0 to  $0.33 \text{ day}^{-1}$  are plotted. Before the binary trend is removed, there are many significant low-frequency signals (blue shaded region), as we would expect from the long-period binary. Once the binary trend is removed, there are no signals with less than 0.01% FAP.

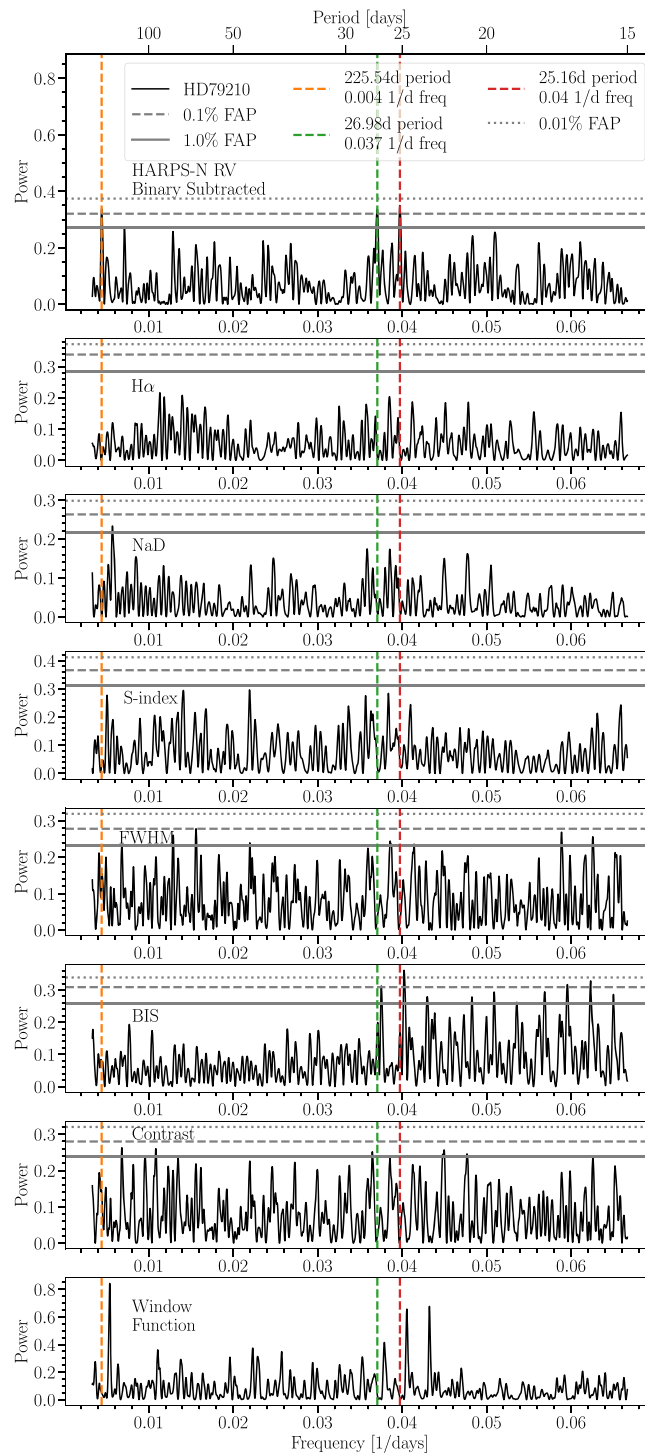


**Figure B4.** Periodograms of HD 79210’s white light HARPS-N radial velocities with the binary trend removed, activity indicators, and the window function. The three most significant peaks ( $<0.1\%$  FAP) are marked with dashed vertical lines. Note that there are no periodic signals in the RVs with FAP  $<0.01\%$ . The 25.16 and 26.98 days signals are just offset from significant ( $<0.01\%$  FAP and  $<0.1\%$  FAP, respectively) peaks in the periodogram of BIS. We suspect that the RV signals correspond to these BIS signals, as BIS signals have been shown to be offset in time from RV variability (Dumusque et al. 2014; Collier Cameron et al. 2019). We suspect that the 225.54 days signal is a harmonic of the 25.16 days variability signal.

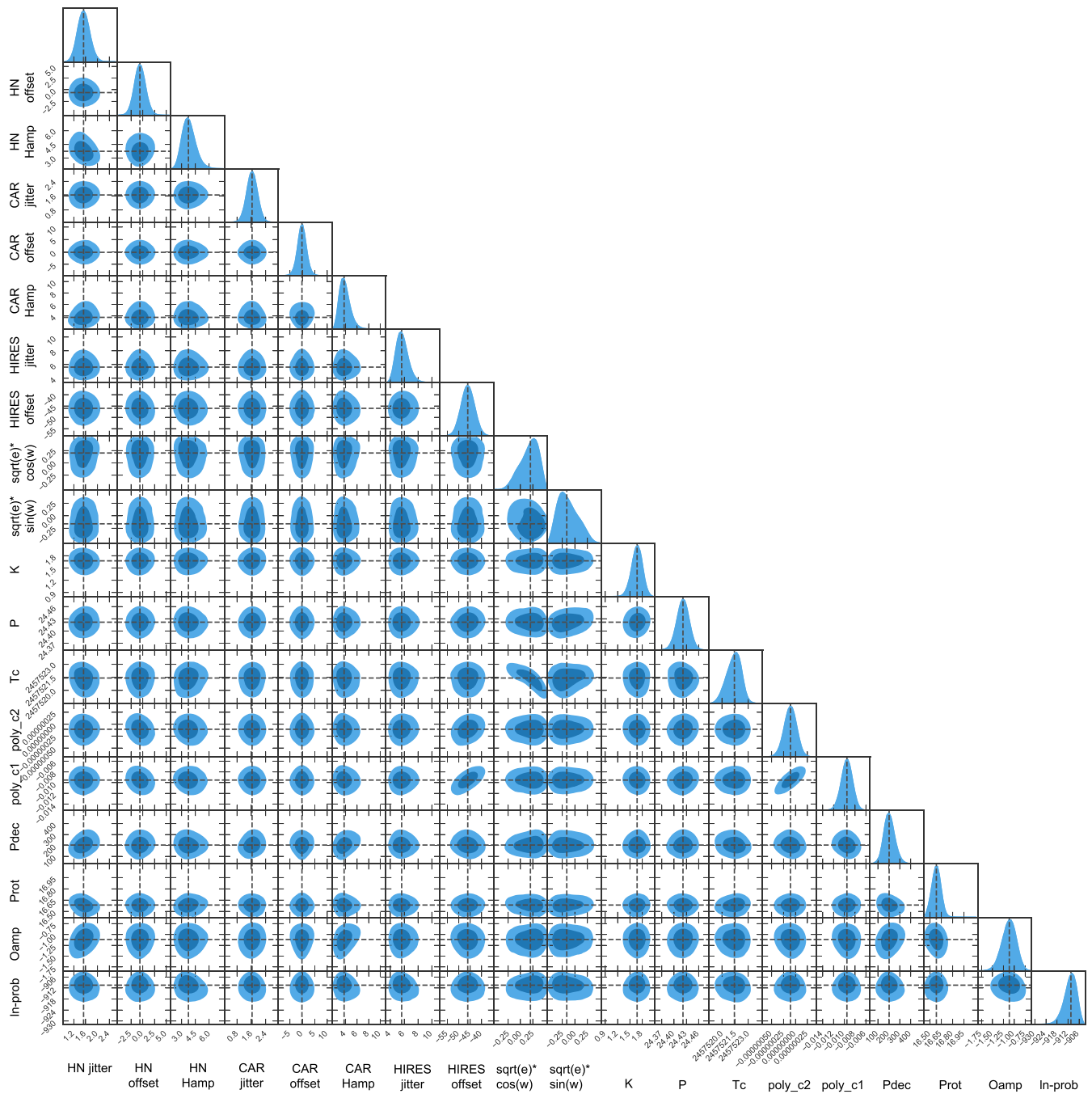


**Figure B5.** Posterior distributions of the free parameters when fitting HD 79211’s combined HARPS-N and CARMENES RV data set with an eccentric orbit and a quasi-periodic GP kernel.



## Appendix C Tables

**Table C1**  
All Available Magnitudes from Survey Photometry for HD 79210 and HD 79211

Survey	Band	HD 79210	HD 79211	Flags
The Hipparcos and Tycho Catalogues (a)	BTmag	9.388 ± 0.03		
The Hipparcos and Tycho Catalogues (a)	VTmag	7.791 ± 0.016		
The Hipparcos and Tycho Catalogues (a)	Hpmag	7.7796 ± 0.0728	7.9664 ± 0.0824	
The Hipparcos and Tycho Catalogues (a)	Vmag	7.64	7.7	
Gaia EDR3 (b)	Gmag	6.976026	7.054455	
Gaia EDR3 (b)	BPmag	7.863408	7.959406	
Gaia EDR3 (b)	RPmag	6.046104	6.112957	
GALEX-DR5 (c)	FUV	19.471 ± 0.166	19.467 ± 0.165	1
GALEX-DR5 (c)	NUV	16.317 ± 0.016	16.35 ± 0.016	1
The Tycho-2 Catalogue (d)	Tycho-2 BT mag	9.412	9.549	
The Tycho-2 Catalogue (d)	Tycho-2 VT mag	7.789	7.882	
2MASS All-Sky Catalog of Point Sources (e)	Jmag	4.889 ± 0.037	4.779 ± 0.174	2,3
2MASS All-Sky Catalog of Point Sources (e)	Hmag	3.987 ± 0.188	4.043 ± 0.206	3
2MASS All-Sky Catalog of Point Sources (e)	Kmag	3.988 ± 0.036	4.136 ± 0.020 "	2,3
The USNO-B1.0 Catalog (f)	B1mag	9.28	9.41	
The USNO-B1.0 Catalog (f)	B2mag	6.85	6.92	
The USNO-B1.0 Catalog (f)	R1mag	8.35	8.46	
The USNO-B1.0 Catalog (f)	R2mag	6.78	6.85	
SDSS DR13 (g)	<i>u</i>	13.529892 ± 0.0379	12.307867 ± 0.0102	4
SDSS DR13 (g)	<i>g</i>	14.218927 ± 0.2757	8.6298 ± 2.83E-04	4
SDSS DR13 (g)	<i>r</i>	14.097498 ± 1.0859	7.2558894 ± 1.33E-04	4
SDSS DR13 (g)	<i>i</i>	13.7924185 ± 1.0859	6.7036 ± 1.68E-04	4
SDSS DR13 (g)	<i>z</i>	11.406796 ± 1.0869	6.7336 ± 6.48E-04	4

**Notes.** We also note the flags associated with these photometry, which denote the extent to which the two sources were blended in the original images. Flags: (1) The object was originally blended with another one; (2) this category includes detections where the goodness-of-fit quality of the profile-fit photometry was very poor; (3) diffraction spike confusion; (4) unclean.

**References.** (a) ESA (1997), (b) Gaia Collaboration (2021), (c) Bianchi et al. (2011), (d) Høg et al. (2000), (e) Cutri et al. (2003), (f) Monet et al. (2003), and (g) Blanton et al. (2017).

**Table C2**  
HD 79211 Radial Velocities and Activity Indicators

Date (JDb – 2.45e6)	RV (m s <sup>-1</sup> )	eRV (m s <sup>-1</sup> )	FWHM	eFWHM	BIS	eBIS	Contrast	eContrast	Smw	eSmw	Ha	eHa	Na	eNa
6285.612891	20.3	0.8	6117.3	8.7	61.8	1.0	34.232862	0.000001	1.869	0.004	0.577	0.001	0.1229	0.0002
6671.615209	8.7	0.3	6029.1	8.5	56.8	1.0	34.624995	0.000001	0.000	0.000	0.551	0.001	0.1257	0.0002
6671.724181	8.7	0.6	6025.1	8.5	58.0	1.1	34.621989	0.000001	0.000	0.000	0.545	0.001	0.1241	0.0002
6672.512178	10.8	0.3	6040.1	8.5	57.7	1.1	34.550935	0.000001	0.000	0.000	0.556	0.001	0.1244	0.0002
6672.609691	12.4	0.4	6133.3	8.7	60.7	0.9	34.136966	0.000001	1.724	0.003	0.558	0.001	0.1243	0.0002
7014.621385	-0.2	0.6	5984.5	8.5	66.2	1.1	35.042534	0.000001	1.498	0.005	0.534	0.001	0.1206	0.0002
7014.732420	-1.8	0.6	5984.8	8.5	68.9	1.0	35.034022	0.000001	1.480	0.004	0.533	0.001	0.1207	0.0002
7018.726754	5.8	0.5	5994.5	8.5	67.2	1.2	34.991576	0.000001	1.437	0.006	0.523	0.001	0.1214	0.0003
7020.717072	2.8	0.6	5990.4	8.5	74.4	1.2	35.018739	0.000001	1.581	0.006	0.540	0.001	0.1199	0.0003
7020.785177	4.9	0.5	5991.4	8.5	72.8	0.9	34.986452	0.000001	1.536	0.004	0.532	0.001	0.1167	0.0002
7044.748325	6.0	0.5	6002.1	8.5	72.3	0.9	34.923610	0.000001	1.561	0.004	0.535	0.001	0.1200	0.0002
7045.530040	3.3	0.5	5998.6	8.5	68.7	1.2	34.967085	0.000001	1.542	0.006	0.545	0.001	0.1217	0.0003
7045.722216	3.8	0.6	5995.6	8.5	68.6	1.3	34.983797	0.000001	1.536	0.007	0.535	0.001	0.1219	0.0003
7046.602067	4.5	0.5	5997.0	8.5	68.1	0.9	34.963493	0.000001	1.518	0.004	0.528	0.001	0.1206	0.0002
7046.737819	4.5	0.4	5995.3	8.5	67.9	0.9	34.966771	0.000001	1.502	0.003	0.532	0.001	0.1197	0.0002
7048.470341	6.0	0.6	5989.9	8.5	62.4	1.3	35.022517	0.000001	1.471	0.007	0.518	0.001	0.1206	0.0003
7048.557574	6.4	0.5	5988.5	8.5	63.3	1.4	35.022603	0.000001	1.474	0.007	0.520	0.001	0.1211	0.0003
7051.507932	14.6	0.5	6006.5	8.5	65.8	1.1	34.896503	0.000001	1.526	0.005	0.531	0.001	0.1218	0.0002
7051.628868	14.2	0.5	6009.1	8.5	65.9	1.0	34.883580	0.000001	1.603	0.004	0.549	0.001	0.1227	0.0002
7052.598236	9.2	0.6	6014.2	8.5	71.9	1.4	34.869929	0.000001	1.546	0.008	0.539	0.001	0.1220	0.0003
7052.673872	9.3	1.0	6004.5	8.5	68.8	2.3	34.884387	0.000001	1.551	0.016	0.535	0.002	0.1228	0.0005
7053.433842	7.3	0.7	6008.7	8.5	72.7	1.5	34.889942	0.000001	1.588	0.009	0.547	0.001	0.1213	0.0003
7053.572232	7.9	0.7	6007.6	8.5	72.1	1.3	34.881916	0.000001	1.612	0.007	0.553	0.001	0.1211	0.0003
7054.587638	9.7	0.5	6009.7	8.5	68.7	0.9	34.781720	0.000001	1.710	0.004	0.560	0.001	0.1235	0.0002
7054.675635	9.5	0.5	6005.7	8.5	70.3	0.9	34.885117	0.000001	1.590	0.003	0.547	0.001	0.1214	0.0002
7106.458292	5.8	0.5	6002.2	8.5	69.3	1.2	34.941747	0.000001	1.434	0.005	0.504	0.001	0.1176	0.0002
7106.581258	5.1	0.5	6005.6	8.5	68.8	1.2	34.936934	0.000001	1.435	0.006	0.500	0.001	0.1165	0.0002
7107.383100	3.7	0.5	5996.2	8.5	71.5	0.8	34.948208	0.000001	1.462	0.003	0.525	0.001	0.1202	0.0002
7107.511736	3.0	0.5	5996.9	8.5	73.1	1.0	34.955592	0.000001	1.452	0.005	0.512	0.001	0.1180	0.0002
7324.740802	2.0	0.7	6013.2	8.5	71.9	1.4	34.906742	0.000001	1.612	0.008	0.537	0.001	0.1240	0.0003
7324.746300	1.5	0.6	6001.4	8.5	71.3	1.4	34.895632	0.000001	1.599	0.008	0.534	0.001	0.1231	0.0003
7325.700001	2.5	0.5	6004.0	8.5	74.8	1.2	34.916968	0.000001	1.549	0.006	0.515	0.001	0.1208	0.0003
7325.705464	2.4	0.6	6003.9	8.5	74.7	1.2	34.925492	0.000001	1.556	0.006	0.518	0.001	0.1209	0.0003
7332.667583	0.6	0.6	5996.4	8.5	67.9	1.0	34.961330	0.000001	1.572	0.005	0.533	0.001	0.1225	0.0002
7332.753053	1.7	0.6	5998.0	8.5	69.0	1.0	34.960201	0.000001	1.542	0.004	0.525	0.001	0.1225	0.0002
7333.681902	1.3	0.4	6001.3	8.5	67.8	0.8	34.925854	0.000001	1.555	0.003	0.540	0.001	0.1245	0.0002
7333.753366	2.0	0.5	6002.1	8.5	69.3	0.8	34.924959	0.000001	1.538	0.003	0.538	0.001	0.1248	0.0002
7334.624478	0.6	0.7	6010.6	8.5	67.6	0.9	34.885663	0.000001	1.598	0.004	0.544	0.001	0.1236	0.0002
7334.727032	2.3	0.7	6009.3	8.5	66.7	0.8	34.888516	0.000001	1.567	0.003	0.533	0.001	0.1224	0.0002
7335.664700	-0.0	0.6	6008.8	8.5	69.4	1.6	34.925364	0.000001	1.553	0.010	0.517	0.001	0.1247	0.0004
7335.751223	-7.1	0.6	6009.7	8.5	68.5	1.0	34.878111	0.000001	1.536	0.004	0.526	0.001	0.1235	0.0002
7379.570185	-1.7	0.6	5993.8	8.5	71.2	1.1	34.968125	0.000001	1.494	0.005	0.506	0.001	0.1207	0.0002
7379.667493	-1.5	0.4	5990.6	8.5	69.7	0.8	34.966462	0.000001	1.494	0.003	0.506	0.001	0.1208	0.0002
7380.564210	0.1	0.6	5992.2	8.5	70.4	1.3	34.972041	0.000001	1.556	0.007	0.517	0.001	0.1217	0.0003
7380.689505	1.0	0.5	5992.5	8.5	67.9	0.9	34.957374	0.000001	1.545	0.004	0.522	0.001	0.1213	0.0002
7381.620483	0.5	0.4	5994.3	8.5	69.8	1.2	34.972357	0.000001	1.522	0.006	0.515	0.001	0.1218	0.0003
7381.708704	1.2	0.3	5994.9	8.5	65.6	0.9	34.942763	0.000001	1.533	0.004	0.521	0.001	0.1225	0.0002
7384.566887	1.8	0.6	6007.8	8.5	68.6	1.0	34.896642	0.000001	1.555	0.005	0.532	0.001	0.1234	0.0002
7384.665722	-0.7	0.5	6005.1	8.5	70.2	1.1	34.899071	0.000001	1.552	0.005	0.531	0.001	0.1240	0.0002
7385.535905	-1.7	0.7	6014.2	8.5	70.7	1.8	34.896648	0.000001	1.592	0.011	0.518	0.001	0.1226	0.0004
7385.677403	-0.3	0.5	6009.3	8.5	68.4	1.2	34.863785	0.000001	1.618	0.006	0.527	0.001	0.1212	0.0002
7407.475529	2.5	0.6	6036.3	8.5	71.0	0.9	34.716908	0.000001	1.686	0.004	0.567	0.001	0.1246	0.0002
7407.717522	2.7	0.5	6037.7	8.5	72.8	0.9	34.710184	0.000001	1.642	0.004	0.556	0.001	0.1248	0.0002
7408.512642	-0.8	0.5	6032.4	8.5	74.3	0.9	34.759374	0.000001	1.637	0.003	0.554	0.001	0.1238	0.0002
7408.706636	-1.2	0.6	6029.6	8.5	80.3	1.2	34.772884	0.000001	1.668	0.006	0.550	0.001	0.1239	0.0003
7409.461119	-1.0	0.6	6018.8	8.5	79.1	0.9	34.791592	0.000001	1.646	0.004	0.555	0.001	0.1237	0.0002
7410.511099	1.6	0.9	6011.7	8.5	79.3	1.6	34.697860	0.000001	1.607	0.009	0.510	0.001	0.1210	0.0004
7411.517177	-5.0	0.6	5992.5	8.5	72.5	1.2	34.905516	0.000001	1.567	0.005	0.517	0.001	0.1209	0.0002
7411.761853	-1.4	0.8	5978.0	8.5	73.1	2.3	34.518417	0.000001	1.507	0.015	0.513	0.001	0.1296	0.0005
7412.515048	3.3	0.5	5992.8	8.5	71.4	0.9	34.934547	0.000001	1.608	0.004	0.520	0.001	0.1192	0.0002
7412.678358	2.9	0.5	5990.6	8.5	71.7	1.1	34.956586	0.000001	1.585	0.005	0.510	0.001	0.1188	0.0002
7459.508092	3.1	0.8	6027.6	8.5	67.0	2.0	34.808038	0.000001	1.622	0.012	0.544	0.002	0.1233	0.0005
7459.612820	2.0	0.8	6025.7	8.5	73.0	1.8	34.792587	0.000001	1.644	0.011	0.544	0.001	0.1231	0.0004

**Table C2**  
(Continued)

Date (JDb – 2.45e6)	RV (m s <sup>-1</sup> )	eRV (m s <sup>-1</sup> )	FWHM	eFWHM	BIS	eBIS	Contrast	eContrast	Smw	eSmw	Ha	eHa	Na	eNa
7460.614946	2.9	0.5	6013.5	8.5	72.7	1.0	34.819873	0.000001	1.554	0.005	0.541	0.001	0.1235	0.0002
7461.556115	2.8	0.6	6010.7	8.5	74.2	1.2	34.852056	0.000001	1.599	0.006	0.539	0.001	0.1231	0.0003
7461.559865	1.9	0.5	6008.2	8.5	72.1	1.2	34.855077	0.000001	1.617	0.006	0.545	0.001	0.1240	0.0003
7461.563661	1.6	0.6	6011.8	8.5	73.1	1.3	34.834035	0.000001	1.617	0.006	0.544	0.001	0.1235	0.0003
7462.570242	1.8	0.7	6005.5	8.5	72.6	1.3	34.894691	0.000001	1.575	0.007	0.545	0.001	0.1228	0.0003
7462.576318	1.7	0.7	6009.3	8.5	71.9	1.3	34.900651	0.000001	1.576	0.007	0.542	0.001	0.1225	0.0003
7463.478321	6.4	0.6	5999.6	8.5	68.9	1.2	34.918489	0.000001	1.537	0.005	0.534	0.001	0.1220	0.0003
7463.483760	5.0	0.6	5998.8	8.5	67.2	1.2	34.933660	0.000001	1.539	0.006	0.531	0.001	0.1222	0.0003
7463.592711	5.2	0.7	6000.1	8.5	67.6	1.5	34.920505	0.000001	1.519	0.008	0.521	0.001	0.1211	0.0004
7463.598243	5.1	0.8	5998.8	8.5	70.1	1.8	34.950547	0.000001	1.519	0.010	0.520	0.001	0.1210	0.0004
7752.639756	0.9	0.8	6023.6	8.5	65.8	1.7	34.820135	0.000001	1.635	0.010	0.530	0.001	0.1273	0.0004
7753.564001	1.3	1.1	6024.4	8.5	69.0	2.8	34.816407	0.000001	1.624	0.020	0.536	0.002	0.1371	0.0006
7753.786752	1.9	0.6	6028.4	8.5	61.5	1.4	34.754533	0.000001	1.652	0.008	0.536	0.001	0.1244	0.0003
8075.656797	-1.4	0.5	6005.1	8.5	71.8	0.9	34.921503	0.000001	1.572	0.003	0.519	0.001	0.1208	0.0002
8119.563946	-3.8	0.9	5995.9	8.5	62.6	1.6	34.942547	0.000001	1.467	0.008	0.515	0.001	0.1201	0.0003
8120.610033	-5.8	0.7	6002.2	8.5	62.6	1.6	34.907409	0.000001	1.480	0.008	0.551	0.001	0.1361	0.0004
8122.652629	-0.7	0.7	5998.8	8.5	65.9	1.3	34.960728	0.000001	1.507	0.005	0.519	0.001	0.1203	0.0003
8143.542711	-5.1	0.7	5983.7	8.5	74.7	1.6	35.038470	0.000001	1.463	0.010	0.506	0.001	0.1191	0.0003
8147.611456	-3.2	0.7	5976.1	8.5	66.9	1.1	35.055493	0.000001	1.390	0.006	0.489	0.001	0.1186	0.0002
8477.691075	-13.5	0.9	6055.6	8.6	78.6	1.5	34.556499	0.000001	1.775	0.007	0.555	0.001	0.1250	0.0003
8477.757699	-13.7	0.8	6064.4	8.6	89.5	2.0	34.565657	0.000001	1.818	0.011	0.570	0.001	0.1267	0.0004
8526.411740	-7.9	0.7	6076.2	8.6	76.5	1.3	34.461290	0.000001	1.881	0.006	0.581	0.001	0.1277	0.0003
8536.630177	0.1	0.7	6042.3	8.5	60.1	1.2	34.635809	0.000001	1.699	0.005	0.532	0.001	0.1236	0.0002
8538.634332	4.9	0.7	6054.7	8.6	65.7	1.2	34.566339	0.000001	1.743	0.006	0.546	0.001	0.1256	0.0003
8805.645794	-3.5	0.9	6029.3	8.5	74.1	1.4	34.783666	0.000001	1.630	0.006	0.516	0.001	0.1250	0.0003
8805.741588	-2.1	0.7	6026.6	8.5	72.6	0.9	34.739513	0.000001	1.623	0.003	0.519	0.001	0.1246	0.0002
8816.605286	-5.7	0.7	6010.7	8.5	73.4	1.2	34.858948	0.000001	1.587	0.005	0.516	0.001	0.1223	0.0002
8816.723732	-6.6	0.9	6017.1	8.5	69.9	1.5	34.879021	0.000001	1.589	0.007	0.511	0.001	0.1229	0.0003
8818.625772	-6.5	0.7	6016.5	8.5	69.0	0.9	34.815676	0.000001	1.643	0.003	0.531	0.001	0.1245	0.0002
8818.749021	-6.4	0.7	6017.3	8.5	67.1	0.9	34.812491	0.000001	1.613	0.003	0.519	0.001	0.1223	0.0002
8830.770218	-4.4	0.8	6031.1	8.5	75.9	2.1	34.753263	0.000001	1.643	0.011	0.521	0.001	0.1253	0.0005
8832.775143	0.9	0.8	6037.4	8.5	86.0	2.7	34.791074	0.000001	1.598	0.015	0.525	0.002	0.1443	0.0007
8841.672974	-2.7	1.5	6024.0	8.5	53.6	4.0	34.995432	0.000001	1.776	0.029	0.539	0.003	0.1596	0.0009
8847.594680	-11.1	0.7	6018.0	8.5	75.5	1.0	34.836482	0.000001	1.573	0.004	0.513	0.001	0.1223	0.0002
8847.756271	-9.0	0.8	6019.6	8.5	75.7	1.0	34.838014	0.000001	1.612	0.004	0.518	0.001	0.1218	0.0002
8854.646741	-3.0	0.8	6008.0	8.5	69.4	0.9	34.899571	0.000001	1.579	0.003	0.543	0.001	0.1257	0.0002
8883.554321	-7.5	1.0	6008.8	8.5	74.6	2.0	34.980193	0.000001	1.619	0.011	0.526	0.001	0.1214	0.0005
8883.640535	-6.1	2.3	6010.4	8.5	67.4	4.8	35.207201	0.000001	1.783	0.041	0.517	0.003	0.1243	0.0010
8887.479981	-4.4	0.7	6005.1	8.5	71.7	0.8	34.894021	0.000001	1.523	0.003	0.497	0.000	0.1184	0.0001
8887.585245	-3.4	0.7	6004.0	8.5	71.6	0.8	34.900044	0.000001	1.547	0.003	0.505	0.000	0.1198	0.0001
8908.546480	-4.2	0.7	6019.9	8.5	68.5	1.0	34.828600	0.000001	1.690	0.004	0.537	0.001	0.1208	0.0002
8908.666000	-5.1	0.6	6020.9	8.5	66.0	1.3	34.832169	0.000001	1.678	0.006	0.535	0.001	0.1193	0.0003
8910.496814	-2.2	0.7	6020.3	8.5	69.4	0.9	34.833626	0.000001	1.625	0.004	0.526	0.001	0.1216	0.0002
8915.453070	-6.7	0.6	6009.5	8.5	71.8	0.8	34.885467	0.000001	1.536	0.003	0.515	0.000	0.1189	0.0002
8915.546282	-9.3	0.8	6011.3	8.5	68.6	1.4	34.935664	0.000001	1.523	0.007	0.508	0.001	0.1187	0.0003
9655.557594	-19.1	0.7	6012.9	8.5	69.6	1.2	34.793949	0.000001	1.679	0.006	0.549	0.001	0.1235	0.0003
9656.551881	-19.9	1.1	6013.2	8.5	70.1	1.5	34.813970	0.000001	1.612	0.008	0.524	0.001	0.1235	0.0003
9658.456802	-19.7	0.9	6014.8	8.5	72.4	1.2	34.825784	0.000001	1.584	0.006	0.521	0.001	0.1227	0.0002
9659.579979	-18.2	0.7	6005.5	8.5	68.6	0.9	34.840340	0.000001	1.605	0.004	0.540	0.001	0.1230	0.0002
9661.603197	-15.8	0.9	6002.3	8.5	64.1	1.8	34.905553	0.000001	1.594	0.012	0.523	0.001	0.1211	0.0004
9662.554508	-13.6	0.8	6003.4	8.5	71.5	1.4	34.893858	0.000001	1.594	0.008	0.518	0.001	0.1209	0.0003

**Note.** RVs as calculated using TERRA, and activity indicators as calculated by the HARPS-N DRS 3.7.

(This table is available in machine-readable form.)

**Table C3**  
 HD 79210 Radial Velocities and Activity Indicators

Date (JDb – 2.45e6)	RV (m s <sup>-1</sup> )	eRV (m s <sup>-1</sup> )	FWHM	eFWHM	BIS	eBIS	Contrast	eContrast	Smw	eSmw	Ha	eHa	Na	eNa
6671.602883	-17.9	0.6	6205.3	8.8	64.7	0.9	34.702755	0.000001	1.715	0.004	0.548	0.001	0.1255	0.0002
6671.712040	-18.3	0.5	6204.8	8.8	64.6	1.1	34.709181	0.000001	1.731	0.005	0.545	0.001	0.1245	0.0002
6672.500523	-20.4	0.4	6202.7	8.8	64.0	0.9	34.709411	0.000001	1.730	0.004	0.543	0.001	0.1237	0.0002
6672.597364	-19.5	0.3	6196.4	8.8	64.6	0.9	34.701540	0.000001	1.735	0.003	0.546	0.001	0.1237	0.0002
6968.679139	-17.4	0.7	6059.3	8.6	65.8	1.3	35.474655	0.000001	1.556	0.007	0.520	0.001	0.1204	0.0003
7014.608861	-19.2	0.7	6078.1	8.6	69.9	1.0	35.392864	0.000001	1.683	0.005	0.539	0.001	0.1228	0.0002
7014.721910	-25.5	0.5	6081.7	8.6	70.6	1.1	35.379604	0.000001	1.689	0.005	0.544	0.001	0.1229	0.0002
7016.648683	-17.1	0.6	6073.7	8.6	68.7	0.9	35.415204	0.000001	1.630	0.004	0.527	0.001	0.1224	0.0002
7016.744011	-18.1	0.6	6076.2	8.6	64.2	1.3	35.436469	0.000001	1.659	0.007	0.533	0.001	0.1229	0.0003
7018.694229	-17.3	0.7	6071.9	8.6	68.9	1.2	35.443635	0.000001	1.701	0.006	0.555	0.001	0.1258	0.0003
7020.676238	-20.7	0.5	6053.7	8.6	71.7	0.9	35.505181	0.000001	1.581	0.004	0.515	0.001	0.1189	0.0002
7020.773116	-19.7	0.5	6052.8	8.6	68.1	0.9	35.509273	0.000001	1.634	0.004	0.519	0.001	0.1174	0.0002
7044.618278	-11.2	0.6	6046.5	8.6	65.1	0.9	35.588323	0.000001	1.540	0.004	0.516	0.001	0.1201	0.0002
7379.547614	-9.9	0.6	6081.2	8.6	67.8	1.3	35.395780	0.000001	1.624	0.007	0.525	0.001	0.1223	0.0003
7379.558946	-11.0	0.5	6083.7	8.6	69.1	1.0	35.365167	0.000001	1.657	0.005	0.532	0.001	0.1226	0.0002
7379.650825	-9.8	0.5	6082.0	8.6	69.3	0.8	35.364910	0.000001	1.613	0.003	0.530	0.001	0.1228	0.0002
7381.632555	-16.3	0.5	6069.3	8.6	75.5	1.0	35.459527	0.000001	1.584	0.005	0.523	0.001	0.1226	0.0002
7381.719966	-15.8	0.5	6068.5	8.6	78.3	1.0	35.473583	0.000001	1.579	0.005	0.521	0.001	0.1224	0.0002
7407.463307	-16.5	0.7	6087.3	8.6	78.5	1.0	35.347004	0.000001	1.657	0.005	0.548	0.001	0.1224	0.0002
7407.705901	-14.6	0.6	6085.3	8.6	76.3	0.9	35.348105	0.000001	1.687	0.004	0.562	0.001	0.1245	0.0002
7411.506298	-23.9	0.7	6080.3	8.6	61.9	1.4	35.292921	0.000001	1.710	0.007	0.546	0.001	0.1253	0.0003
7411.628022	-15.4	0.8	6073.3	8.6	53.6	1.8	34.952576	0.000001	1.632	0.010	0.538	0.001	0.1362	0.0004
7458.514008	-11.5	0.7	6072.9	8.6	69.6	1.1	35.445024	0.000001	1.589	0.005	0.530	0.001	0.1224	0.0003
7458.519656	-11.9	0.7	6069.2	8.6	67.8	1.2	35.447314	0.000001	1.605	0.006	0.531	0.001	0.1226	0.0003
7458.594999	-11.8	0.7	6069.1	8.6	71.8	1.1	35.452089	0.000001	1.663	0.005	0.549	0.001	0.1237	0.0003
7458.600508	-11.2	0.6	6069.7	8.6	68.3	1.1	35.444495	0.000001	1.651	0.006	0.547	0.001	0.1237	0.0003
7462.478835	-14.8	0.7	6078.5	8.6	63.9	1.1	35.442927	0.000001	1.626	0.005	0.534	0.001	0.1219	0.0002
7462.484310	-14.5	0.6	6075.8	8.6	65.5	1.1	35.439044	0.000001	1.628	0.005	0.533	0.001	0.1214	0.0002
7723.698932	-8.7	0.8	6069.4	8.6	72.2	1.9	35.488947	0.000001	1.593	0.011	0.548	0.002	0.1394	0.0005
7732.568598	-6.0	0.6	6066.9	8.6	66.4	1.1	35.454995	0.000001	1.681	0.005	0.545	0.001	0.1217	0.0002
7732.575995	-5.2	0.5	6068.3	8.6	67.0	1.1	35.455369	0.000001	1.685	0.005	0.543	0.001	0.1211	0.0002
7732.732312	-6.2	0.5	6069.2	8.6	67.7	0.8	35.427932	0.000001	1.648	0.003	0.539	0.000	0.1225	0.0001
7752.629201	-6.5	0.8	6070.5	8.6	65.9	1.5	35.467998	0.000001	1.730	0.009	0.553	0.001	0.1278	0.0004
7753.542357	-7.3	1.0	6071.2	8.6	56.4	2.4	35.480444	0.000001	1.613	0.016	0.520	0.002	0.1358	0.0006
7753.774564	-3.8	0.6	6074.2	8.6	64.6	1.2	35.429545	0.000001	1.674	0.006	0.536	0.001	0.1237	0.0003
7764.562994	-10.8	0.7	6094.4	8.6	56.8	1.5	35.267229	0.000001	1.679	0.008	0.548	0.001	0.1280	0.0004
7817.518062	-7.9	0.6	6094.8	8.6	67.5	1.2	35.290803	0.000001	1.717	0.006	0.539	0.001	0.1215	0.0003
8075.643996	2.6	0.6	6125.3	8.7	66.3	0.9	35.088364	0.000001	1.823	0.003	0.557	0.001	0.1261	0.0002
8086.621865	-0.5	0.8	6092.6	8.6	65.5	1.9	35.338213	0.000001	1.692	0.012	0.530	0.001	0.1294	0.0004
8120.622082	-1.0	0.8	6112.7	8.6	69.1	1.8	35.180743	0.000001	1.742	0.010	0.569	0.001	0.1415	0.0004
8121.702763	-1.3	0.7	6108.6	8.6	70.2	1.5	35.197757	0.000001	1.776	0.008	0.544	0.001	0.1273	0.0003
8122.640152	2.3	0.7	6105.8	8.6	69.4	1.2	35.174412	0.000001	1.834	0.006	0.560	0.001	0.1263	0.0003
8142.664448	4.6	1.2	6118.9	8.7	69.7	3.3	35.097965	0.000001	1.838	0.033	0.543	0.002	0.1314	0.0007
8143.527815	-3.6	0.6	6114.1	8.6	66.2	1.7	35.142612	0.000001	1.802	0.012	0.553	0.001	0.1259	0.0004
8143.646565	-1.9	1.1	6126.8	8.7	67.6	2.4	35.101413	0.000001	1.904	0.018	0.561	0.002	0.1283	0.0005
8147.598157	3.2	0.7	6140.6	8.7	71.1	1.1	34.965033	0.000001	1.876	0.007	0.585	0.001	0.1273	0.0002
8239.368652	6.1	0.4	6103.9	8.6	66.4	0.9	35.225081	0.000001	1.668	0.004	0.543	0.001	0.1224	0.0002
8454.691049	12.6	0.5	6126.2	8.7	68.3	0.9	35.053999	0.000001	1.778	0.003	0.551	0.001	0.1273	0.0002
8454.736712	12.1	0.6	6126.0	8.7	68.6	1.0	35.057840	0.000001	1.789	0.004	0.544	0.001	0.1267	0.0002
8526.425177	5.0	1.2	6144.3	8.7	83.4	2.4	35.034133	0.000001	1.968	0.014	0.593	0.002	0.1282	0.0005
8536.616161	13.5	0.6	6111.9	8.6	56.2	1.0	35.167891	0.000001	1.735	0.005	0.532	0.001	0.1247	0.0002
8538.621890	10.0	0.6	6136.6	8.7	66.9	1.1	35.008712	0.000001	1.854	0.005	0.562	0.001	0.1256	0.0002
8544.459923	-0.4	0.6	6116.8	8.7	82.0	0.9	35.109791	0.000001	1.858	0.003	0.565	0.001	0.1242	0.0002
8544.595796	-0.5	0.7	6117.2	8.7	84.5	1.0	35.143497	0.000001	1.780	0.005	0.546	0.001	0.1226	0.0002
8545.458728	-3.2	0.7	6098.3	8.6	82.3	1.1	35.239870	0.000001	1.737	0.005	0.528	0.001	0.1218	0.0002
8545.572797	-0.8	0.6	6095.5	8.6	80.0	1.0	35.231555	0.000001	1.781	0.004	0.536	0.001	0.1213	0.0002
8546.411967	0.8	0.7	6086.8	8.6	75.8	1.4	35.331340	0.000001	1.708	0.007	0.525	0.001	0.1210	0.0003
8546.513687	2.1	0.5	6083.9	8.6	75.4	1.1	35.317667	0.000001	1.723	0.005	0.533	0.001	0.1223	0.0002
8548.397384	2.2	0.9	6066.5	8.6	67.4	1.4	35.421875	0.000001	1.652	0.008	0.508	0.001	0.1179	0.0003
8816.630520	12.3	1.0	6082.9	8.6	68.2	2.7	35.492177	0.000001	1.815	0.018	0.540	0.002	0.1337	0.0006
8818.637903	6.4	0.7	6081.4	8.6	74.0	0.9	35.367111	0.000001	1.688	0.003	0.527	0.001	0.1245	0.0002
8841.694745	13.8	1.1	6126.3	8.7	70.1	2.4	35.303118	0.000001	1.862	0.015	0.557	0.002	0.1371	0.0006
8843.649122	8.9	0.8	6120.0	8.7	70.0	1.3	35.200034	0.000001	1.883	0.006	0.572	0.001	0.1280	0.0003

**Table C3**  
(Continued)



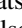

Date (JDb – 2.45e6)	RV (m s <sup>-1</sup> )	eRV (m s <sup>-1</sup> )	FWHM	eFWHM	BIS	eBIS	Contrast	eContrast	Smw	eSmw	Ha	eHa	Na	eNa
8847.607122	7.8	0.5	6116.3	8.6	75.4	1.1	35.215659	0.000001	1.813	0.005	0.553	0.001	0.1249	0.0002
8847.769535	7.7	0.6	6112.1	8.6	73.6	0.9	35.215072	0.000001	1.895	0.004	0.574	0.001	0.1249	0.0002
8854.634287	9.0	0.6	6094.6	8.6	64.1	0.9	35.308292	0.000001	1.762	0.003	0.567	0.001	0.1284	0.0002
8861.624299	16.1	0.8	6117.1	8.7	71.8	1.1	35.214263	0.000001	1.806	0.005	0.545	0.001	0.1241	0.0002
8861.707136	14.6	0.7	6113.0	8.6	70.8	0.9	35.198146	0.000001	1.795	0.004	0.537	0.001	0.1227	0.0002
8883.567735	15.6	1.0	6088.7	8.6	75.0	1.7	35.455835	0.000001	1.721	0.009	0.533	0.001	0.1215	0.0004
8887.493210	11.7	0.6	6098.0	8.6	67.3	0.9	35.326083	0.000001	1.735	0.003	0.528	0.001	0.1214	0.0002
8887.596530	13.0	0.7	6097.9	8.6	67.8	0.9	35.313566	0.000001	1.750	0.003	0.538	0.001	0.1227	0.0002
8899.553769	11.8	0.7	6093.7	8.6	72.3	1.0	35.331840	0.000001	1.725	0.004	0.533	0.001	0.1210	0.0002
8908.534212	15.5	0.6	6117.8	8.7	64.7	0.9	35.174930	0.000001	1.829	0.004	0.551	0.001	0.1219	0.0002
8908.651325	16.2	0.6	6119.5	8.7	67.8	1.1	35.199129	0.000001	1.791	0.005	0.548	0.001	0.1225	0.0002
8910.484569	13.5	0.6	6121.2	8.7	72.1	0.9	35.157370	0.000001	1.795	0.004	0.557	0.001	0.1239	0.0002
8915.440466	13.7	0.6	6096.9	8.6	74.5	0.8	35.285193	0.000001	1.763	0.003	0.543	0.001	0.1211	0.0002
8915.533771	11.6	0.5	6088.2	8.6	77.4	1.2	35.348770	0.000001	1.721	0.006	0.533	0.001	0.1212	0.0003
9656.565329	16.8	0.9	6063.3	8.6	62.0	1.3	35.432578	0.000001	1.693	0.007	0.529	0.001	0.1235	0.0003
9658.443411	18.9	0.8	6079.5	8.6	65.7	1.3	35.369161	0.000001	1.702	0.008	0.529	0.001	0.1241	0.0003
9659.567838	16.5	0.8	6078.8	8.6	68.7	0.8	35.317963	0.000001	1.740	0.004	0.543	0.001	0.1243	0.0002
9670.406369	13.2	0.7	6067.5	8.6	68.3	0.9	35.399315	0.000001	1.742	0.004	0.544	0.001	0.1229	0.0002

**Note.** RVs as calculated using TERRA, and activity indicators as calculated by the HARPS-N DRS 3.7.

(This table is available in machine-readable form.)

### ORCID iDs

Victoria DiTomasso  <https://orcid.org/0000-0003-0741-7661>  
 Chantanelle Nava  <https://orcid.org/0000-0001-8838-3883>  
 Mercedes López-Morales  <https://orcid.org/0000-0003-3204-8183>  
 Allyson Bieryla  <https://orcid.org/0000-0001-6637-5401>  
 Ryan Cloutier  <https://orcid.org/0000-0001-5383-9393>  
 Luca Malavolta  <https://orcid.org/0000-0002-6492-2085>  
 Annelies Mortier  <https://orcid.org/0000-0001-7254-4363>  
 Lars A. Buchhave  <https://orcid.org/0000-0003-1605-5666>  
 Keivan G. Stassun  <https://orcid.org/0000-0002-3481-9052>  
 Alessandro Sozzetti  <https://orcid.org/0000-0002-7504-365X>  
 Aldo Stefano Bonomo  <https://orcid.org/0000-0002-6177-198X>  
 David Charbonneau  <https://orcid.org/0000-0002-9003-484X>  
 Andrew Collier Cameron  <https://orcid.org/0000-0002-8863-7828>  
 Rosario Cosentino  <https://orcid.org/0000-0003-1784-1431>  
 Mario Damasso  <https://orcid.org/0000-0001-9984-4278>  
 Xavier Dumusque  <https://orcid.org/0000-0002-9332-2011>  
 A. F. Martínez Fiorenzano  <https://orcid.org/0000-0002-4272-4272>  
 Adriano Ghedina  <https://orcid.org/0000-0003-4702-5152>  
 R. D. Haywood  <https://orcid.org/0000-0001-9140-3574>  
 David Latham  <https://orcid.org/0000-0001-9911-7388>  
 Emilio Molinari  <https://orcid.org/0000-0002-1742-7735>  
 Matteo Pinamonti  <https://orcid.org/0000-0002-4445-1845>  
 Ennio Poretti  <https://orcid.org/0000-0003-1200-0473>  
 Ken Rice  <https://orcid.org/0000-0002-6379-9185>  
 Dimitar Sasselov  <https://orcid.org/0000-0001-7014-1771>

Manu Stalport  <https://orcid.org/0000-0003-0996-6402>  
 Stéphane Udry  <https://orcid.org/0000-0001-7576-6236>  
 Christopher Watson  <https://orcid.org/0000-0002-9718-3266>  
 Thomas G. Wilson  <https://orcid.org/0000-0001-8749-1962>

### References

- Alonso-Floriano, F. J., Morales, J. C., Caballero, J. A., et al. 2015, *A&A*, **577**, A128  
 Anglada-Escude, G., & Butler, R. P. 2012, *ApJS*, **200**, 15  
 Belokurov, V., Penoyre, Z., Oh, S., et al. 2020, *MNRAS*, **496**, 1922  
 Benedict, G. F., Henry, T. J., Franz, O. G., et al. 2016, *AJ*, **152**, 141  
 Bergfors, C., Brandner, W., Daemgen, S., et al. 2013, *MNRAS*, **428**, 182  
 Bianchi, L., Herald, J., Efremova, B., et al. 2011, *Ap&SS*, **335**, 161  
 Blanton, M. R., Bershady, M. A., Abolfathi, B., et al. 2017, *AJ*, **154**, 28  
 Boyajian, T. S., von Braun, K., van Belle, G., et al. 2012, *ApJ*, **757**, 112  
 Brandt, T. D. 2021, *ApJS*, **254**, 42  
 Buchhave, L. A., Latham, D. W., Johansen, A., et al. 2012, *Natur*, **486**, 375  
 Buchhave, L. A., Bizzarro, M., Latham, D. W., et al. 2014, *Natur*, **509**, 593  
 Butler, R. P., Vogt, S. S., Laughlin, G., et al. 2017, *AJ*, **153**, 208  
 Carter, J. A., Winn, J. N., Holman, M. J., et al. 2011, *ApJ*, **730**, 82C  
 Chaplin, W. J., Cegla, H. M., Watson, C. A., Davies, G. R., & Ball, W. H. 2019, *AJ*, **157**, 163  
 Christian, S., Vanderburg, A., Becker, J., et al. 2022, *AJ*, **163**, 207  
 Collier Cameron, A., Mortier, A., Phillips, D., et al. 2019, *MNRAS*, **487**, 1082  
 Collins, K. A., Kielkopf, J. F., Stassun, K. G., & Hessman, F. V. 2017, *AJ*, **153**, 77  
 Cortes-Contreras, M., Bejar, V. J. S., Caballero, J. A., et al. 2016, *yCat*, **597**, A47  
 Cosentino, R., Lovis, C., Pepe, F., et al. 2012, *Proc. SPIE*, **8446**, 84461V  
 Cosentino, R., Lovis, C., Pepe, F., et al. 2014, *Proc. SPIE*, **9147**, 91478C  
 Cutri, R. M., Skrutskie, M. F., van Dyk, S., et al. 2003, *yCat*, II/246  
 Desidera, S., & Barbieri, M. 2007, *A&A*, **462**, 345  
 Doyle, L. R., Carter, J. A., Fabrycky, D. C., et al. 2011, *Sci*, **333**, 1602  
 Dressing, C. D., & Charbonneau, D. 2015, *ApJ*, **807**, 45  
 Dumusque, X., Boisse, I., & Santos, N. C. 2014, *ApJ*, **796**, 132D  
 Dumusque, X., Udry, S., Lovis, C., Santos, N. C., & Monteiro, M. J. P. F. G. 2011, *A&A*, **525**, A140  
 ESA 1997, The Hipparcos and Tycho Catalogues  
 Fulton, B. J., Petigura, E. A., Blunt, S., & Sinukoff, E. 2018, *PASP*, **130**, 044504

- Gaia Collaboration, Brown, A. G. A., Vallenari, A., et al. 2021, *A&A*, **649**, A1
- Gaia Collaboration, Brown, A. G. A., Vallenari, A., et al. 2012, arXiv:2012.01533
- Gaia Collaboration, Prusti, T., de Bruijne, J. H. J., et al. 2016, *A&A*, **595**, A1
- Glebocki, R., & Gnacinski, P. 2005, in 13th Cambridge Workshop on Cool Stars, Stellar Systems and the Sun, ed. F. Favata, G. A. J. Hussain, & B. Battrick (Paris: European Space Agency), 571
- González-Álvarez, E., Zapatero Osorio, M. R., Caballero, J. A., et al. 2020, *A&A*, **637**, A93
- Haywood, R. D., Vanderburg, A., Mortier, A., et al. 2018, *AJ*, **155**, 203
- Henry, T., Jao, W.-C., Subasavage, J., et al. 2006, *AJ*, **132**, 2360
- Høg, E., Fabricius, C., Makarov, V. V., et al. 2000, *A&A*, **355**, L27
- Jain, C., Paul, B., Sharma, R., Jaleel, A., & Dutta, A. 2017, *MNRAS*, **468**, L118
- Jeffers, S. V., & Keller, C. U. 2009, in AIP Conf. Proc. 1094, COOL STARS, STELLAR SYSTEMS AND THE SUN (Melville, NY: AIP), 664
- Kervella, P., Arenou, F., & Thévenin, F. 2022, *A&A*, **657**, A7
- Kirkpatrick, J. D., Henry, T. J., & McCarthy, D. W., Jr. 1991, *ApJS*, **77**, 417
- Kochanek, C. S., Shappee, B. J., Stanek, K. Z., et al. 2017, *PASP*, **129**, 10450
- Kraus, A. L., Ireland, M. J., Huber, D., Mann, A. W., & Dupuy, T. J. 2016, *AJ*, **152**, 17
- Lindgren, L., Hernández, J., Bombrun, A., et al. 2018, *A&A*, **616**, A2
- Lindgren, L., Klioner, S. A., Hernández, J., et al. 2021, *A&A*, **649**, A2
- Malavolta, L. 2016, Astrophysics Source Code Library, ascl:1612.008
- Mann, A. W., Feiden, G. A., Gaidos, E., Boyajian, T., & Braun, K. v. 2015, *ApJ*, **804**, 64
- Marzari, F., & Thebault, P. 2019, arXiv:2002.12006
- Mayor, M., Pepe, F., Queloz, D., et al. 2003, *Msngr*, **114**, 20
- Merline, W. J., & Howell, S. B. 1995, *ExA*, **6**, 163
- Monet, D. G., Levine, S. E., Canzian, B., et al. 2003, *AJ*, **125**, 984
- Mortier, A., & Collier Cameron, A. 2017, *A&A*, **601**, A110
- Mortier, A., Zapatero Osorio, M. R., Malavolta, L., et al. 2020, *MNRAS*, **499**, 5004
- Morton, T. D. 2015, VESPA: False positive probabilities calculator, Astrophysics Source Code Library, ascl:1503.010
- Motalebi, F., Udry, S., Gillon, M., et al. 2015, *A&A*, **584**, A72
- Mugrauer, M., & Neuhauser, R. 2009, *A&A*, **494**, 373
- Oliphant, T. E. 2007, *CSE*, **9**, 10
- Orosz, J. A., Welsh, W. F., Carter, J. A., et al. 2012, *Sci*, **337**, 1511
- Pepe, F., Lovis, C., Ségransan, D., et al. 2011, *A&A*, **534**, A58
- Pollacco, D., Skillen, I., Cameron, A., et al. 2006, *Ap&SS*, **304**, 253
- Quirrenbach, A., Amado, P. J., Caballero, J. A., et al. 2016, *Proc. SPIE*, **9908**, 990812
- Reiners, A., Zechmeister, M., Caballero, J. A., et al. 2018, *A&A*, **612**, A49
- Ribas, I., Morales, J. C., Jordi, C., et al. 2008, *MmSAI*, **79**, 562
- Ricker, G. R., Winn, J. N., Vanderspek, R., et al. 2015, *JATIS*, **1**, 014003
- Roell, T., Neuhauser, R., Seifahrt, A., & Mugrauer, M. 2012, *A&A*, **542**, A92
- Sarmiento, P., Rojas-Ayala, B., Delgado Mena, E., & Blanco-Cuaresma, S. 2021, *A&A*, **649**, A147
- Schwamb, M. E., Orosz, J. A., Carter, J. A., et al. 2013, *ApJ*, **768**, 127S
- Schweitzer, A., Passegger, V. M., Cifuentes, C., et al. 2019, *A&A*, **625**, A68
- Shappee, B. J., Prieto, J. L., Grupe, D., et al. 2014, *ApJ*, **788**, 48
- Stassun, K. G., & Torres, G. 2016, *AJ*, **152**, 180
- Stassun, K. G., & Torres, G. 2021, *ApJL*, **907**, L33
- Susemihl, N., & Meyer, M. R. 2022, *A&A*, **657**, A48
- Szentgyorgyi, A. H., Geary, J. G., Latham, D. W., et al. 2005, *BAAS*, **207**, 110.10
- Price-Whelan, A. M., Sipocz, B. M., Gunther, H. M., et al. 2018, *AJ*, **156**, 123
- Thebault, P., & Haghighipour, N. 2015, in Planetary Exploration and Science: Recent Results and Advances, ed. S. Jin, N. Haghighipour, & W.-H. Ip (Berlin: Springer), 309
- Vogt, S. S., Allen, S. L., Bigelow, B. C., et al. 1994, *Proc. SPIE*, **2198**, 362
- Ward-Duong, K., Patience, J., De Rosa, R. J., et al. 2015, *MNRAS*, **449**, 2618
- Winters, J. G., Henry, T. J., Jao, W.-C., et al. 2019, *AJ*, **157**, 216